

The relation of H₂CO, ¹²CO, and ¹³CO in molecular clouds^{*}

Xin. Di. Tang^{1,2}, Jarken. Esimbek^{1,3}, Jian. Jun. Zhou^{1,3}, Gang. Wu^{1,3}, Wei. Guang. Ji^{1,2}, and Daniel. Okoh^{1,4}

¹ Xinjiang Astronomical Observatory, Chinese Academy of Sciences, Urumqi 830011, PR China
e-mail: tangxindi@xao.ac.cn

² Graduate University of the Chinese Academy of Sciences, Beijing 100080, PR China

³ Key Laboratory of Radio Astronomy, Chinese Academy of Sciences, Urumqi 830011, PR China

⁴ Physics & Astronomy Department, University of Nigeria, Nsukka 410001, Nigeria

Received / Accepted

ABSTRACT

Aims. We seek to understand how the 4.8 GHz formaldehyde absorption line is distributed in the MON R2, S156, DR17/L906, and M17/M18 regions. More specifically, we look for the relationship among the H₂CO, ¹²CO, and ¹³CO spectral lines.

Methods. The four regions of MON R2 (60' × 90'), S156 (50' × 70'), DR17/L906 (40' × 60'), and M17/M18 (70' × 80') were observed for H₂CO (beam 10'), H110α recombination (beam 10'), 6 cm continuum (beam 10'), ¹²CO (beam 1'), and ¹³CO (beam 1'). We compared the H₂CO, ¹²CO, ¹³CO, and continuum distributions, and also the spectra line parameters of H₂CO, ¹²CO, and ¹³CO. Column densities of H₂CO, ¹³CO, and H₂ were also estimated.

Results. We found out that the H₂CO distribution is similar to the ¹²CO and the ¹³CO distributions on a large scale. The correlation between the ¹³CO and the H₂CO distributions is better than between the ¹²CO and H₂CO distributions. The H₂CO and the ¹³CO tracers systematically provide consistent views of the dense regions. Their maps have similar shapes, sizes, peak positions, and molecular spectra and present similar central velocities and line widths. Such good agreement indicates that the H₂CO and the ¹³CO arise from similar regions.

Key words. interstellar medium: molecular clouds – interstellar medium: molecules – stars: formation

1. INTRODUCTION

The H₂CO distribution in the Galaxy has been noted by Davies & Few (1979). They found that the H₂CO distribution is similar to that of H II and CO. Downes et al. (1980) surveyed 262 Galactic radio sources using the H₂CO absorption line at 4.830 GHz, and H110α recombination line at 4.874 GHz, and found that H₂CO is associated with most of the H II regions. It is a good probe of the star formation region. H₂CO absorption is only seen in absorption against the background continuum, and it gives different constraints to mm and sub-mm spectral lines, which are seen both in front of and behind the H II region. It provides a unique probe of the physical conditions for the foreground cloud. Comparative surveys of H₂CO absorption and CO emission in the galactic center have been reported by Scoville et al. (1972, 1973) and Solomon et al. (1972). A good correlation is generally found between H₂CO and CO. Cohen et al. (1983) generally found good agreement on a large scale but a connection that does not have enough detail. Recently, Rodríguez et al. (2006, 2007) and Zhang et al. (2012) compared the H₂CO absorption and CO emission profiles towards the Galactic anti-center, and the following five regions, L1204/S140, W49, W3, DR21/W75, and NGC2024/NGC2023. They found a crude correlation between these two molecular tracers on a large scale. Generally, the ¹²CO (1–0) emission line is optically thick, and the H₂CO (1₁₀–1₁₁) absorption line is optically thin, so the two lines have many different properties in the dense region. The

¹³CO (1–0) emission line is optically thin, and it can trace dense region ($n(\text{H}_2) > 10^3 \text{ cm}^{-3}$). It is therefore similar to H₂CO.

Liszt & Lucas (1995) compared N(H₂CO) with N(HCO⁺) and N(¹³CO) towards compact extragalactic mm-wave continuum sources, and found that H₂CO has a rapid increase with N(HCO⁺), but not as rapid as that of N(¹³CO). N(¹³CO) is strongly affected by fractionation (Liszt & Lucas 1998), so that the H₂CO–¹³CO comparison is perhaps interesting, while it is not directly used in deciphering the general chemistry. Cohen et al. (1983) compared the H₂CO (beam ~ 10') with ¹³CO (beam ~ 8') maps in the Orion molecular cloud and found that the agreement between H₂CO and ¹³CO is considerably better, but with different relative intensities and with minor differences in the detailed morphology. Therefore, making a point-by-point comparison will be interesting when the ¹³CO profiles become available. In this paper, we report new CO, H₂CO, 6 cm continuum and H110α observations in four Galactic HII regions of MON R2, S156, DR17/L906, and M17/M18. We are interested in making a comparative study of the H₂CO, ¹²CO, and ¹³CO lines.

2. OBSERVATIONS

2.1. Formaldehyde, H110α recombination, and continuum

From September 2010 to August 2011, we observed the H₂CO line, the H110α line, and the 6 cm continuum with the Nanshan 25 m radio telescope of Xinjiang Astronomical Observatory. The 25 m radio telescope has an HPBW (half power beam width) of 10' at 4829.6594 MHz. A 6 cm low noise receiver was

^{*} Appendices are only available in electronic form at <http://www.aanda.org>.

used. The system temperature was about 23 K during observations. Digital autocorrelation spectrometers were used with 4096 channels and 80 MHz bandwidth, and a corresponding velocity resolution of 1.206 km s^{-1} . The line detection limit is about 23 mK with 10 min integration time. To get the higher signal/noise ratio, each point's total integration time ranged from 30 min to several hours. The continuum at 4.8 GHz were processed with a bandwidth of about 400 MHz, and the error was approximately 5%. The DPFU (degrees per flux unit) value was 0.116 K Jy^{-1} . The pointing and tracking accuracy was better than $15''$, and the beam efficiency was 65%. The observation was performed in the so-called ON/OFF mode. A diode noise source was used to calibrate the spectrum and the flux error was 15%.

2.2. Carbon monoxide

From 15 to 26 May 2011, the ^{12}CO and ^{13}CO observations of the four regions were carried out with the 13.7 m millimeter wave telescope of Purple Mountain Observatory in Delingha. The 3 mm cryogenically cooled 9 – beam SIS (Superconductor Insulator Superconductor) receiver was used in double sideband mode, and the system temperatures ranged from 105 to 140 K during the observations. Using the fast Fourier transform spectrometer, the ^{12}CO velocity resolution was 0.16 km s^{-1} , while the ^{13}CO velocity resolution was 0.17 km s^{-1} . The rms was about 0.1 K at 1 min integration time, and the line detection limit about 0.15 K. The three CO lines were observed simultaneously. The HPBW was $60''$ at 110 GHz. The grid spacing of mapping observations was $30''$, and the pointing accuracy was better than $10''$. The average integration time of every point was one minute. The source was mapped using the on-the-fly mode of observation. The standard source W51 was checked roughly every two hours.

3. RESULTS

3.1. Data reduction and exhibition

Data reduction for H_2CO , $\text{H}110\alpha$, ^{12}CO , and ^{13}CO lines were done using CLASS and GREG, which are parts of GILDAS¹. To enhance comparison with the observation, we smoothed the ^{12}CO and ^{13}CO observations to $10''$, and resampled them on the H_2CO observing grid. Sources observed are shown in Table B.1. The $\text{H}110\alpha$ data are reported in Table B.2. The parameters of the H_2CO and the 6 cm continuum are reported in Table B.3, while ^{12}CO and ^{13}CO data are reported in Table B.4. The H_2CO , $\text{H}110\alpha$, ^{12}CO , and ^{13}CO line spectra are shown in Fig.B.1. Line integral intensities of H_2CO , ^{12}CO , and ^{13}CO for four sources are shown in Figs.1, A.1, and A.3. Continuum and $\text{H}110\alpha$ distributions are shown in Fig.A.5.

The H_2CO ($1_{10}-1_{11}$) apparent peak optical depth was determined using a simply standard radiative transfer result, $\tau_{app} = -\ln[1 + T_L/(T_c + 2.73 - T_{ex})]$, where T_L is the antenna temperature in K, T_c is the continuum brightness temperature in K, and T_{ex} is the excitation temperature of the $1_{10}-1_{11}$ transition of H_2CO . The excitation temperature T_{ex} values are in the range of 1.5 to 2.0 K (Heiles 1973, Vanden Bout et al. 1983, Young et al. 2004). Here we use a mean value of $T_{ex} = 1.7 \text{ K}$. The column density of H_2CO at rotational state 1_{11} was obtained from the apparent peak optical depth using $N(\text{H}_2\text{CO}) = 9.4 \times 10^{13} \cdot \tau_{app} \cdot \Delta V$ (Pipenbrink & Wendker 1988), where ΔV is the FWHM in km s^{-1} . The difference between our assumed value of T_{ex} and the one used

¹ GILDAS package was developed by IRAM (Institute de Radioastronomie Millimétrique). <http://www.iram.fr/IRAMFR/GILDAS>.

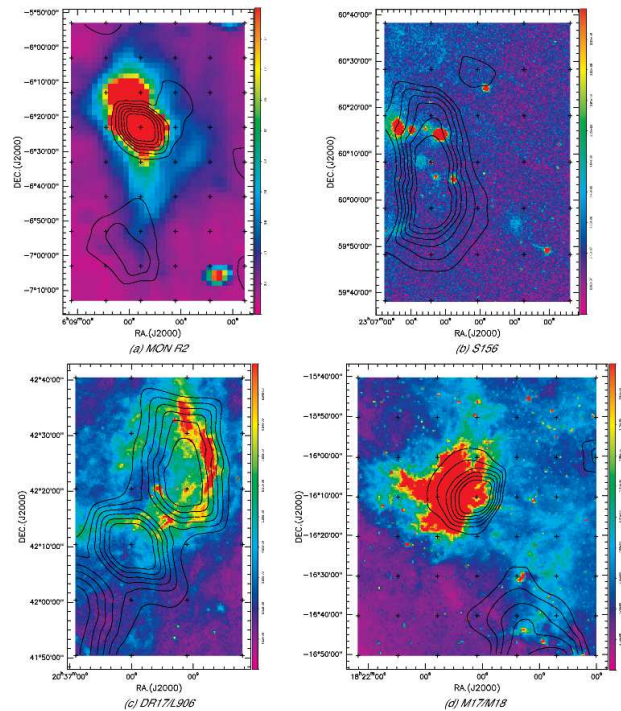


Fig. 1. Contours and color-scale maps of integrated area toward (a) MON R2, (b) S156, (c) DR17/L906, and (d) M17/M18. The contour and color-scale map respectively represent the integrated intensities of the H_2CO and the mid-infrared $8.28 \mu\text{m}$ MSX emission in S156, DR17/L906, and M17/M18 regions. For the MON R2 region, the color-scale map represents the IRAS $12 \mu\text{m}$ data. (a) For the MON R2 region: contour levels are -0.17 to -0.46 in steps of $-0.06 \text{ K km s}^{-1}$. (b) For the S156 region: contour levels are -0.09 to -0.25 in steps of $-0.03 \text{ K km s}^{-1}$. (c) For the DR17/L906 region: contour levels are -0.12 to -0.32 in steps of $-0.04 \text{ K km s}^{-1}$. (d) For the M17/M18 region: contour levels are -0.42 to -1.11 in steps of $-0.14 \text{ K km s}^{-1}$.

in deriving the constant in the above expression (2.0 K) results in an offset of less than 0.1 dex in Fig.5. And the H_2 column density was obtained using the relation $N(\text{H}_2\text{CO})/N(\text{H}_2) = 1.25 \times 10^{-9}$ (Few & Booth 1979, Scoville & Solomon 1973, Evans et al. 1975). The local thermodynamic equilibrium (LTE) electron temperature T_e^* was estimated following Brown et al. (1978) and Pipenbrink & Wendker (1988). The optical depths of ^{13}CO and the column densities of both ^{13}CO and H_2 were estimated using Sato (1994) calculations, on the assumption that the cloud is in LTE.

3.2. Description of sources

MON R2. – The size of MON R2 observed is about $60' \times 90'$. The $\text{H}110\alpha$ line was not detected. Maps of the integrated intensities of the H_2CO , ^{12}CO , and ^{13}CO line velocities range from 0 to 20 km s^{-1} . There is a velocity gradient of several km s^{-1} for H_2CO , ^{12}CO , and ^{13}CO across the cloud. The spectrum of intensity peaks of H_2CO shows two velocity components at 7.6 and 10.52 km s^{-1} . The velocity component at 10.52 km s^{-1} agrees with the intensity peaks of the ^{12}CO and ^{13}CO lines.

S156. – About $50' \times 70'$ of this region have been observed. We did not detect the $\text{H}110\alpha$ line. The line widths in the central part of the cloud are $\sim 3.8 \text{ km s}^{-1}$, more than twice the width normally measured in the dark clouds. This suggests that the cloud could be affected by the H II region. Maps of integrated

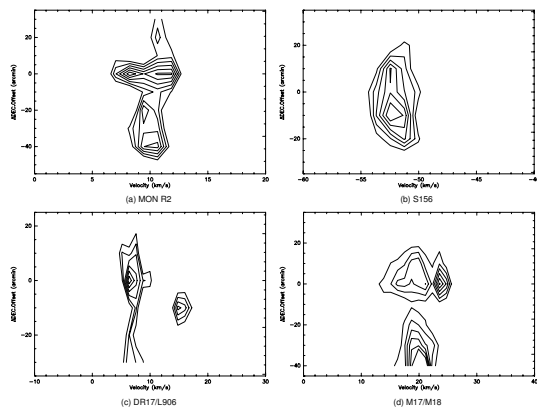


Fig. 2. Position-velocity diagrams of H₂CO for (a) MON R2 and (b) S156, regions along DEC. for $\Delta\alpha = 0$, for (c) DR17/L906 region from offset (20, -30) to (-10, 20), and (d) M17/M18 region from offset (-30, -40) to (0, 30). For the MON R2, S156, and DR17/L906 regions: contour levels are -0.03 to -0.08 in steps of -0.01 K. For the M17/M18 region: contour levels are -0.03 to -0.18 in steps of -0.03 K.

intensities of H₂CO, ¹²CO, and ¹³CO line velocities range from -55 to -45 km s⁻¹. There is a velocity gradient of several km s⁻¹ for H₂CO, ¹²CO, and ¹³CO across the cloud. The velocity of the H₂CO intensity peak is -50.28 km s⁻¹, which agrees with those of the ¹²CO and ¹³CO emission lines.

DR17/L906. – The size of our observed region is about 40'×60'. The strong H110 α emission was detected in the DR17 region with an average velocity of 11.4 km s⁻¹. Maps of the integrated intensities of the H₂CO, ¹²CO and ¹³CO line velocities range from -10 to 20 km s⁻¹. The H₂CO average spectrum shows two velocity components at 6.3 and 14.9 km s⁻¹. The velocity component at 6.3 km s⁻¹ of the H₂CO agrees with those of the DR17 H II region and the continuum emission. This is nearly half of the velocity of the H110 α recombination line. The ¹²CO and ¹³CO average spectrum shows three velocity components at -1.6, 6.0, and 13.8 km s⁻¹. The ¹²CO and ¹³CO velocity components at 13.8 km s⁻¹ and the H₂CO velocity component at 14.9 km s⁻¹ are associated with the L906 region.

M17/M18. – About 70'×80' region have been observed. It covers the M17 region and north of M18. Nine H110 α recombination lines were detected in the M17 region with an average velocity of 16.4 km s⁻¹. Maps of the integrated intensities of the H₂CO, ¹²CO and ¹³CO line velocities range from 10 to 50 km s⁻¹. The H₂CO average spectrum shows three velocity components at 18.3, 22.4, and 37.6 km s⁻¹. The ¹²CO and ¹³CO average spectrum shows four velocity components at 20.0, 28.2, 38.3, and 57.8 km s⁻¹. The H₂CO velocity component 18.3 km s⁻¹ agrees with the velocity component at 20.0 km s⁻¹ of the ¹²CO and ¹³CO, which also agrees with the H II region in M17. The H₂CO cloud distribution, line temperatures, and narrow line width comparing with values observed in the dark cloud shows that the cloud has been negatively influenced by the H II region for the velocity component at 22.4 km s⁻¹. The H₂CO velocity component at 37.6 km s⁻¹ agrees with the 38.3 km s⁻¹ value for the ¹²CO and ¹³CO lines.

4. DISCUSSION

We mapped four regions for the H₂CO, ¹²CO, and ¹³CO (Figs.1, A.1, and A.3). The maps show that the distribution of H₂CO is similar to ¹²CO and ¹³CO on a scale of 2 ~ 10 pc. The position-

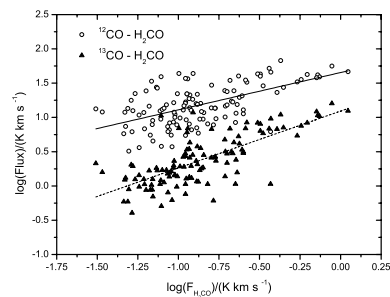


Fig. 3. Correlation between the H₂CO line flux and ¹²CO, ¹³CO line flux at corresponding points in MON R2, S156, DR17/L906, and M17/M18. The solid line is the linear fit for H₂CO and ¹²CO flux data, and the dashed line is the linear fit for H₂CO and ¹³CO.

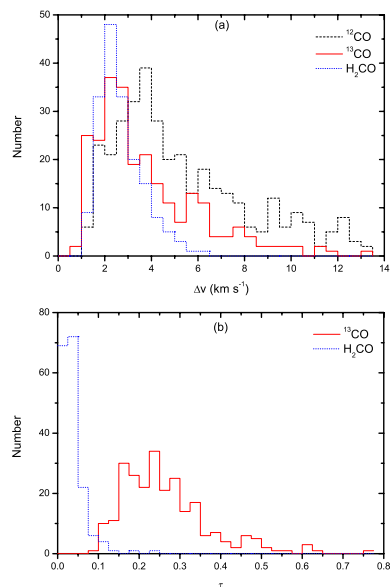


Fig. 4. (a) Histogram showing the measured widths for H₂CO, ¹²CO, and ¹³CO. (b) Histogram showing the histogram of the peak optical depths of H₂CO and ¹³CO distribution. Parts of H₂CO data are selected from Zhang et al. (2012).

velocity diagrams toward four regions (Figs.2, A.2, and A.4) also show that the H₂CO velocity agrees well with ¹²CO and ¹³CO. This suggests that H₂CO is directly related to the CO, and not merely located along the same line of sight. These indicate that in large-scale H₂CO can trace warm regions like ¹²CO and ¹³CO. The H₂CO is better correlated with the ¹³CO than with the ¹²CO especially in the Mon R2, S156, L906, and M17/M18 regions. The DR17 region shows a prominent feature that the ¹²CO and ¹³CO are not as strong as H₂CO. Toward four regions, the ¹²CO, ¹³CO, and H₂CO cloud distribution ranges gradually decrease with these three molecules. The H₂CO maps agree well with the IR maps toward the Mon R2 and DR17 regions. Towards the M17 region, the H₂CO intensity peak is at about 10' (~4 pc) offset from the 8.28 μ m MSX peak. The H₂CO absorption probably has no relation with the MSX emission in the S156 region.

The relation between H₂CO fluxes and those of ¹²CO and ¹³CO are shown in Fig.3. The best-fitted straight lines are $\log(F_{12CO}) = (0.54 \pm 0.07)\log(F_{H_2CO}) + (1.65 \pm 0.07)$ (K km s⁻¹) and $\log(F_{13CO}) = (0.83 \pm 0.07)\log(F_{H_2CO}) + (1.09 \pm 0.07)$ (K km s⁻¹). The equations show that F_{H_2CO} is linearly well cor-

related with F_{12CO} and F_{13CO} ; the correlation coefficients are 0.58 and 0.73. The good relation between F_{H_2CO} and F_{13CO} is an indication that the H_2CO and ^{13}CO lines are located in similar environments.

Statistical histograms of the Gaussian fitting widths of H_2CO , ^{12}CO , and ^{13}CO (Fig.4 (a)) shows that the H_2CO line width range is from 1.2 to 8.5 $km\ s^{-1}$, and the average line width $\langle\Delta V(H_2CO)\rangle$ is 2.5 $km\ s^{-1}$. All the H_2CO line widths observed exceed the thermal line widths 0.3 $km\ s^{-1}$. The thermal line widths for ^{12}CO and ^{13}CO is about 0.2 $km\ s^{-1}$, which is lower than all the ^{12}CO and ^{13}CO line widths observed. In addition, the widest hyperfine structure components of the H_2CO line are separated by about 0.8 $km\ s^{-1}$ (Young et al. 2004, Troscompt et al. 2009). This is less than our velocity resolution. The contribution of hyperfine structure broadening and thermal broadening to the measured H_2CO line widths is therefore likely to be small to moderate. Ninety percent of H_2CO line widths are distributed in the range of $\Delta V(H_2CO) < 4\ km\ s^{-1}$, and the distribution range of $\Delta V(H_2CO)$ is less than for ^{12}CO and ^{13}CO . The main distributions and average line widths of H_2CO and ^{13}CO are similar. There are no obvious correlations between the line widths of H_2CO , ^{12}CO , and ^{13}CO . The frequency distribution of the peak optical depths of H_2CO and ^{13}CO spectra (Fig.4 (b)) shows that nearly all the H_2CO optical depths are lower than those of ^{13}CO . The average optical depth of H_2CO is $\langle\tau(H_2CO)\rangle \sim 0.037$, which can be compared to the value 0.055 quoted by Downes et al. (1980) for 262 galactic radio sources. The fairly low optical depth indicates that the H_2CO spectra is optically thin in almost all the regions observed.

The correlation between H_2CO and ^{13}CO peak column density (Fig.5) shows that the H_2CO peak column density range is $1.1 \times 10^{12} - 6.3 \times 10^{13}\ cm^{-2}$, which is similar to the value range quoted by Federman et al. (1990) for the dense interstellar clouds. The column density corresponds to the MON R2, S156, L906, and M17 H_2CO intensity peak positions, and parts of M18 northern region are distributed in a box of the range $N(H_2CO) < 1.7 \times 10^{13}\ cm^{-2}$ and $N(^{13}CO) > 4.7 \times 10^{15}\ cm^{-2}$, which shows a lack of H_2CO . With the exception of this box, the remaining data points show a strong correlation, and the best fit slope is $N(H_2CO)/N(^{13}CO) = (4.1 \pm 0.2) \times 10^{-3}$. The $N(H_2CO)/N(^{13}CO)$ ratio against offset position towards four regions (Fig.6) shows that the $N(H_2CO)/N(^{13}CO)$ ratios increase from the center to the edge regions of the molecular cloud where the $N(H_2CO)/N(^{13}CO)$ ratio increases about two to three times.

5. CONCLUSIONS

We observed and mapped large areas in four regions of MON R2, S156, DR17/L906, and M17/M18 using the H_2CO ($1_{10-1_{11}}$) absorption, H110 α recombination, 6 cm continuum, ^{12}CO ($1-0$), and ^{13}CO ($1-0$) emissions. The H_2CO distributions are similar to ^{12}CO and ^{13}CO distributions in four regions, with the ^{13}CO distribution better correlated with the H_2CO distributions than the ^{12}CO distribution. The H_2CO and ^{13}CO tracers systematically provide consistent views of the dense regions, in which their maps have similar shapes, sizes, peak positions, and molecular spectra, presenting similar central velocities and line widths. Such good agreement indicates that the H_2CO absorption and the ^{13}CO emission lines both arise in similar regions. The H_2CO and ^{13}CO column density ratio $N(H_2CO)/N(^{13}CO)$ changes with different $n(H_2)$ density regions in the molecular cloud. From the center to the edges of the molecular cloud, the $N(H_2CO)/N(^{13}CO)$ ratio jumps about two to three times.

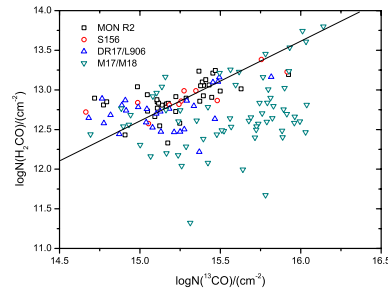


Fig. 5. Correlation between the H_2CO and ^{13}CO peak column density. Straight line is the best-fit line for the source outside the range of $N(H_2CO) < 1.7 \times 10^{13}\ cm^{-2}$ and $N(^{13}CO) > 4.7 \times 10^{15}\ cm^{-2}$.

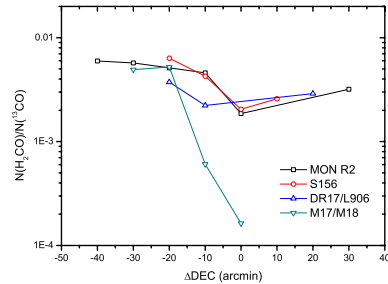


Fig. 6. Derived H_2CO and ^{13}CO peak column density ratio $N(H_2CO)/N(^{13}CO)$ against position along DEC. for $\Delta\alpha = 0$ towards the MON R2, S156, and M17 regions. Towards DR17/L906 region $\Delta\alpha = 10$.

Acknowledgements. We thank all the staff of Nanshan Observatory and Delingha of Purple Mountain Observatory for observations. And we thank Z. B. Jiang, Z. W. Chen, and J. Y. Li for providing the CO data of the M17/M18 region. This work was funded by The National Natural Science foundation of China under grant 10778703, and partly supported by the China Ministry of Science and Technology under State Key Development Program for Basic Research (2012CB821800) and The National Natural Science foundation of China under grant 10873025.

References

- Brown, J. C., Robertson, M. N., & Canfield, R. C. 1978, *SoPh*, 57, 399
Cohen, R. J., Matthews, N., Few, R. W., & Booth, R. S. 1983, *MNRAS*, 203, 1123
Davies, R. D., & Few, R. W. 1979, *IAUS*, 84, 81
Downes, D., Wilson, T. L., Bieging, J., & Wink, J. 1980, *A&AS*, 40, 379
Evans, N. J., II, Morris, G., Sato, T., Zuckerman, B. 1975, *ApJ*, 96, 433
Federman, S. R., Huntress, W. T., Jr., & Prasad, S. S. 1990, *ApJ*, 354, 504
Few, R. W., & Booth, R. S. 1979, *MNRAS*, 188, 181
Heiles, C. 1973, *ApJ*, 183, 441
Herbst, W., & Racine, R. 1976, *AJ*, 81, 840
Hoglund, B., & Gordon, M. A. 1973, *ApJ*, 182, 45
Liszt, H. S., & Lucas, R. 1995, *A&A*, 299, 847
Liszt, H. S., & Lucas, R. 1998, *A&A*, 339, 561
Pipenbrink, A., & Wendker, H. J. 1988, *A&A*, 191, 313
Rodríguez, M. I., Allen, R., Loinard, L., & Wiklind, T. 2006, *ApJ*, 652, 1230
Rodríguez, M. I., Wiklind, T., Allen, R., Escalante, V., & Loinard, L. 2007, *ApJ*, 663, 824
Sato, F., Mizuno, A., Nagahama, T., Onishi, T., Yonekura, Y., & Fukui, Y. 1994, *ApJ*, 435, 279
Scoville, N. Z., & Solomon, P. M. 1973, *ApJ*, 180, 31
Scoville, N. Z., Solomon, P. M., & Thaddeus, P. 1972, *ApJ*, 172, 335
Solomon, P. M., Scoville, N. Z., Penzias, A. A., Wilson, R. W., & Jefferts, K. B. 1972, *ApJ*, 178, 125
Troscompt, N., Faure, A., Maret, S., Ceccarelli, C., Hily-Blant, P., & Wiesenfeld, L. 2009, *A&A*, 506, 1243
Vanden Bout, P. A., Snell, R. L., & Wilson, T. L. 1983, *A&A*, 118, 337
Young, K., Lee, J., Evans, N., Goldsmith, P., & Doty, S. 2004, *ApJ*, 614, 252
Zhang, C. P., Esimbek, J., Zhou, J. J., Wu, G., & Du, Z. M. 2012, *Ap&SS*, 337, 283

Appendix A: The ^{12}CO , ^{13}CO and continuum maps

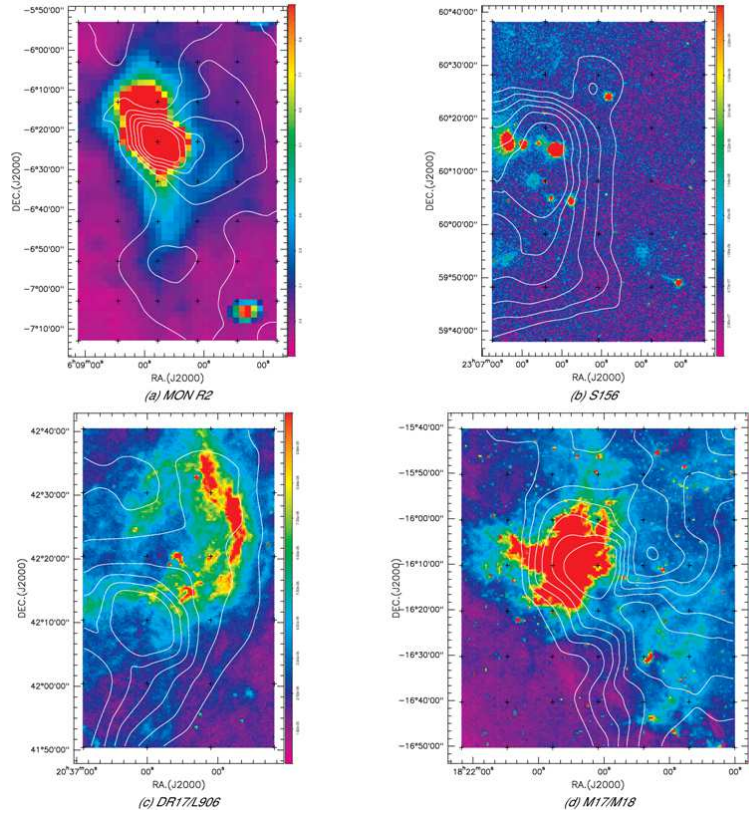


Fig. A.1. The integrated intensities of the ^{12}CO maps of integrated area toward (a) MON R2, (b) S156, (c) DR17/L906, and (d) M17/M18. The color-scale maps are the same as Fig.1. (a) For the MON R2 region: ^{12}CO contour levels are from 12.80 to 34.14 in steps of 4.27 K km s $^{-1}$. (b) For the S156 region: ^{12}CO contour levels are from 12.63 to 33.69 in steps of 4.21 K km s $^{-1}$. (c) For the DR17/L906 region: ^{12}CO contour levels are from 12.72 to 39.26 in steps of 4.91 K km s $^{-1}$. (d) For the M17/M18 region: ^{12}CO contour levels are from 29.34 to 78.24 in steps of 9.78 K km s $^{-1}$.

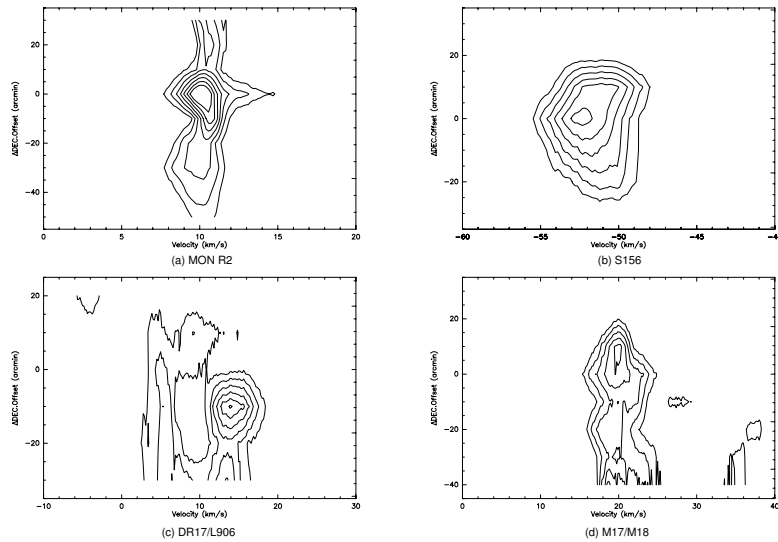


Fig. A.2. Position-velocity diagrams of ^{12}CO for (a) MON R2, (b) S156, (c) DR17/L906, and (d) M17/M18. The positions for ^{12}CO are the same as Fig.2. For the MON R2, S156, and M17/M18 regions, contour levels are 3 to 8 in steps of 1 K. Contour levels are 1.3 to 6.3 in steps of 1 K for the DR17/L906 region.

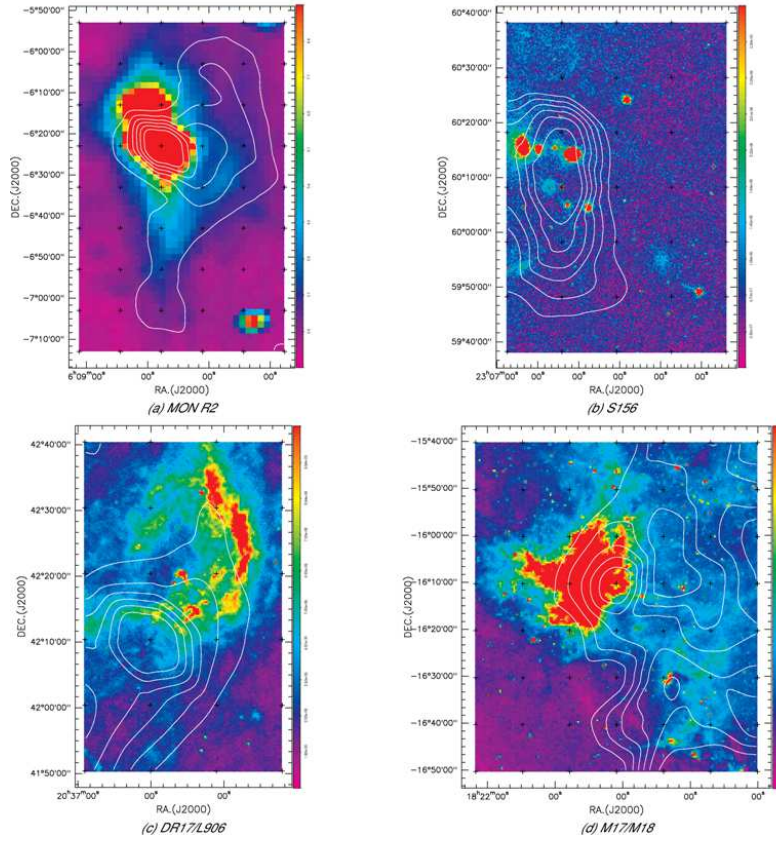


Fig. A.3. The integrated intensities of the ^{13}CO maps of integrated area toward (a) MON R2, (b) S156, (c) DR17/L906, and (d) M17/M18. The color-scale maps are the same as Fig.1. (a) For the MON R2 region: ^{13}CO contour levels are from 2.66 to 7.10 in steps of 0.89 K km s^{-1} . (b) For the S156 region: ^{13}CO contour levels are from 2.53 to 6.76 in steps of 0.84 K km s^{-1} . (c) For the DR17/L906 region: ^{13}CO contour levels are from 2.64 to 7.05 in steps of 0.88 K km s^{-1} . (d) For the M17/M18 region: ^{13}CO contour levels are from 7.83 to 20.89 in steps of 2.61 K km s^{-1} .

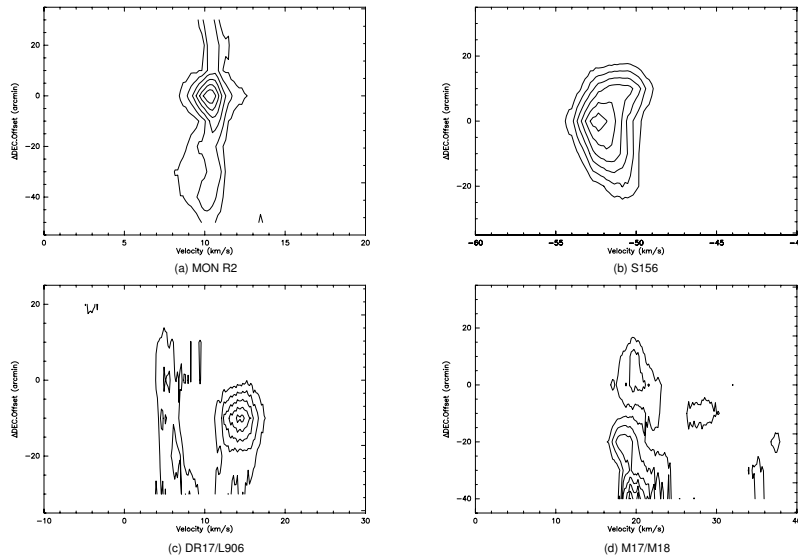


Fig. A.4. Position-velocity diagrams of ^{13}CO for (a) MON R2, (b) S156, (c) DR17/L906, and (d) M17/M18. The positions for ^{13}CO are the same as in Fig.2. (a) For the MON R2 region: contour levels are 0.5 to 3 in steps of 0.5 K. (b) For the S156 region: contour levels are 0.6 to 2.1 in steps of 0.3 K. (c) For the DR17/L906 region: contour levels are 0.3 to 1.8 in steps of 0.3 K. (d) For the M17/M18 region: contour levels are 0.8 to 3.8 in steps of 0.5 K.

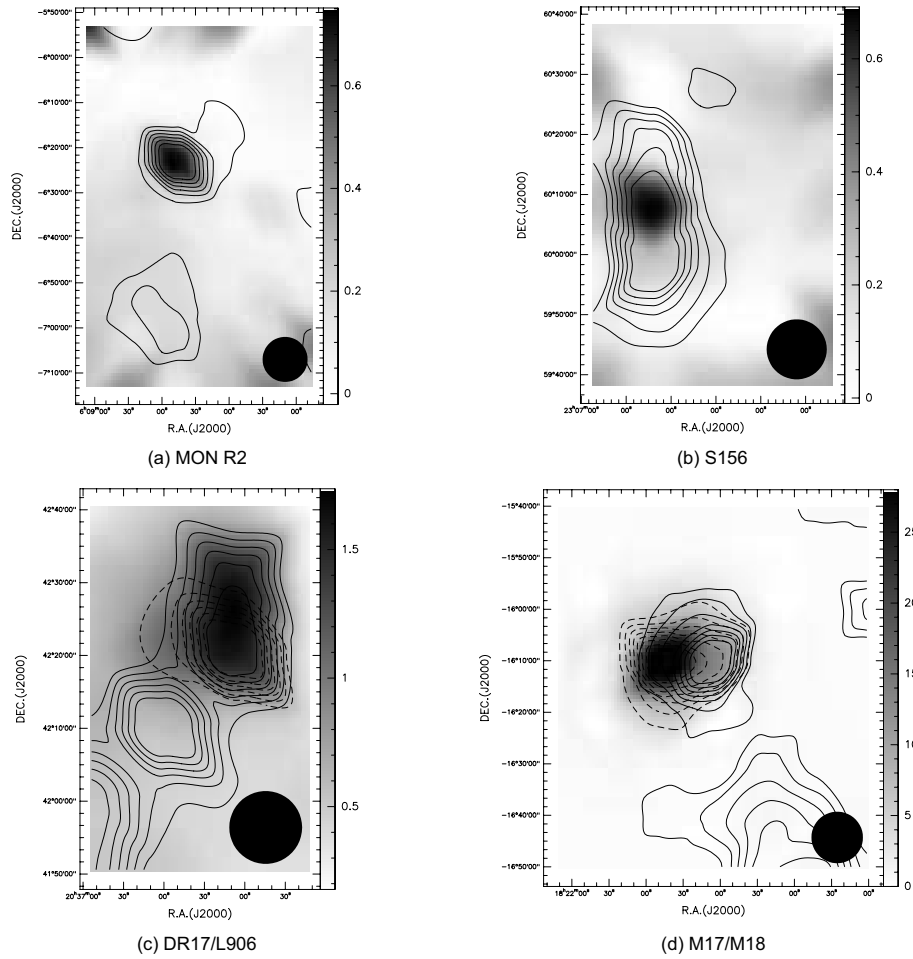


Fig. A.5. Location of the radio continuum emission (gray scale) overlaid on the H₂CO observation lines (black contour lines) and H110 α emission lines (dash contour lines) toward (a) MON R2, (b) S156, (c) DR17/L906, and (d) M17/M18. H₂CO contour levels are the same as Fig.1 for four regions. For the DR17/L906 region: H110 α contour levels are 0.67, 0.89, 1.11, 1.33, 1.56, and 1.78 K km s⁻¹; for the M17/M18 region: H110 α contour levels are 2.91, 4.36, 5.81, 7.26, 8.72, 10.17, and 11.62 K km s⁻¹. The gray bars are given in units of K.

Appendix B: Line parameters and spectra

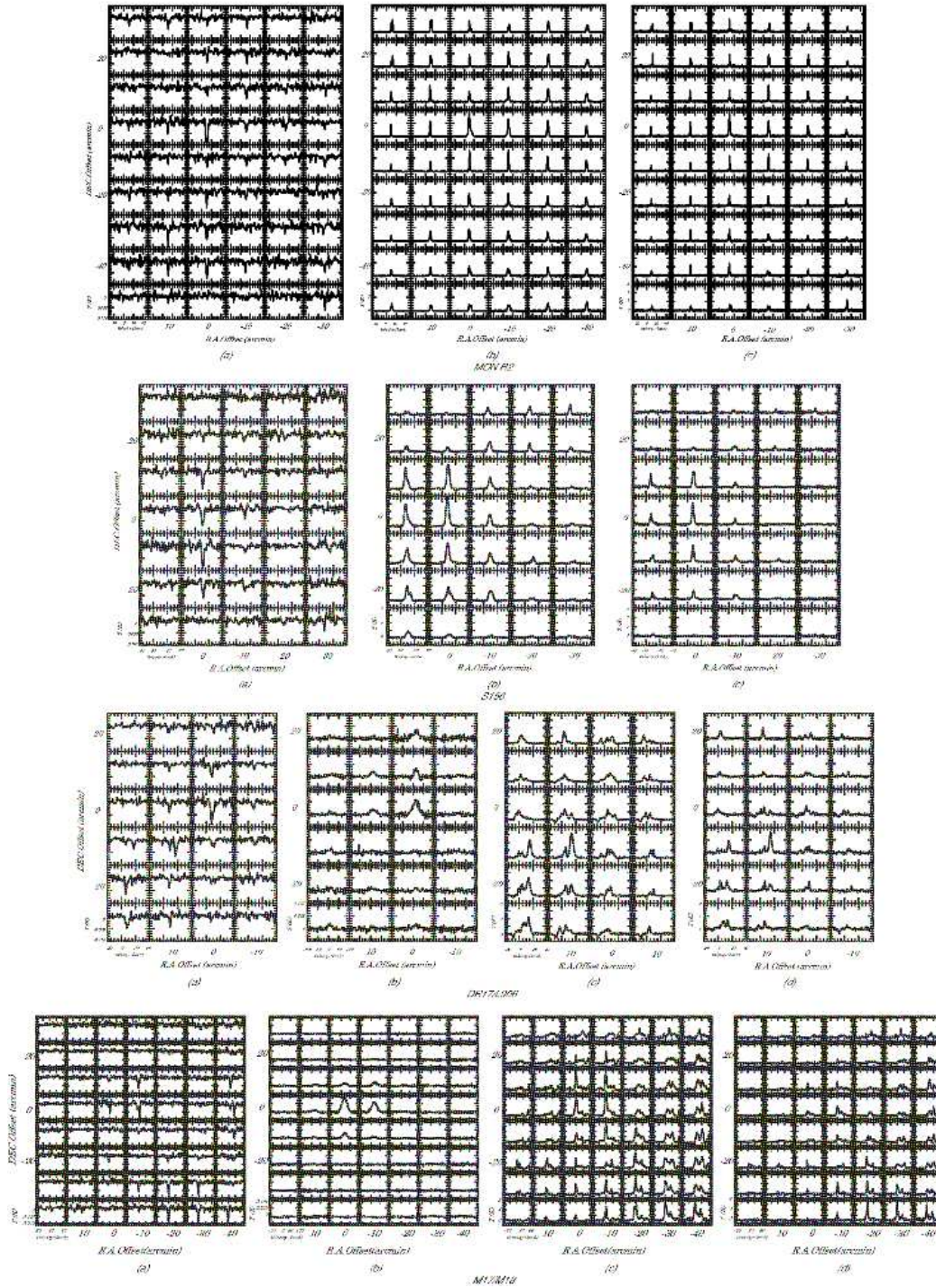


Fig. B.1. The spectra of (a) H_2CO , (b) ^{12}CO , and (c) ^{13}CO lines toward MON R2 and S156 regions. And the spectra of (a) H_2CO , (b) $\text{H}110\alpha$, (c) ^{12}CO , and (d) ^{13}CO lines toward DR17/L906 and M17/M18 regions.

Table B.1. Source positions.

Sources	R.A.(J2000) (^h ^m ^s)	DEC.(J2000) ([°] ['] ^{''})	Size($\alpha \times \delta$) (arcmin ²)	References
MON R2	06:07:46.60	-06:22:59.0	60'×90'	(1)
S156	23:05:24.80	60:08:14.0	50'×70'	(2)
DR17/L906	20:35:06.16	42:20:23.7	40'×60'	(3)
M17/M18	18:20:47.11	-16:10:17.5	70'×80'	(4)

References. (1) Herbst & Racine (1976); (2) Hoglund & Gordon (1973); (3) Schneider et al. (2006); (4) Downes et al. (1980).

Table B.2. Parameters of the H110 α recombination line.

Sources	Offset (arcmin)	Flux (K km s ⁻¹)	Velocity (km s ⁻¹)	Width (km s ⁻¹)	T _L (K)	T _C (K)	T _e [*] (K)
DR17/L906	0, 0	2.04(0.11)	12.7(0.8)	31.5(1.9)	0.06	1.63	8154
	0, 10	0.70(0.06)	14.7(0.9)	18.2(1.6)	0.04	1.61	20320
M17/M18	0, 0	14.40(0.20)	17.5(0.2)	34.6(0.4)	0.39	31.1	19187
	-10, 0	9.91(0.25)	17.7(0.4)	34.9(1.0)	0.27	13.9	13176
	-10, -10	1.24(0.08)	17.2(0.8)	26.6(1.8)	0.04	0.95	7894
	0, -10	3.89(0.10)	19.2(0.3)	25.6(0.8)	0.14	6.58	15539
	10, -10	1.35(0.14)	19.0(1.4)	50.0(1.4)	0.03	1.34	9846
	10, 0	1.92(0.10)	17.2(0.9)	32.7(2.2)	0.06	2.36	11745
	10, 10	1.17(0.09)	22.3(1.2)	31.1(2.8)	0.04	1.81	14405
	0, 10	2.72(0.13)	18.8(0.8)	33.1(1.9)	0.08	5.96	19368
-10, 10	2.72(0.13)	20.1(0.7)	29.2(1.5)	0.09	4.99	16669	

Notes. Parameters listed concern the simultaneously observed the H110 α recombination line.

Table B.3. Parameters of the H₂CO (1₁₀–1₁₁) absorption line.

Sources	Offset (arcmin)	Flux (K km s ⁻¹)	Velocity (km s ⁻¹)	Width (km s ⁻¹)	T _L (K)	T _C (K)
MON R2	0, 0	-0.30(0.04)	7.6(0.2)	2.6(0.3)	-0.11	0.74
		-0.24(0.04)	10.5(0.1)	1.9(0.4)	-0.12	
	-10, 0	-0.21(0.03)	10.7(0.3)	3.8(0.8)	-0.05	
	-10, -10	-0.13(0.02)	10.6(0.2)	2.2(0.5)	-0.05	0.09
	0, -10	-0.15(0.03)	9.7(0.3)	2.5(0.5)	-0.06	0.14
	10, -10	-0.08(0.02)	9.3(0.1)	1.2(1.6)	-0.06	0.19
	10, 0	-0.15(0.03)	9.1(0.2)	1.9(0.6)	-0.07	0.16
	10, 10	-0.05(0.02)	9.9(0.2)	1.2(0.8)	-0.04	0.04
	0, 10	-0.09(0.02)	10.5(0.1)	1.2(0.4)	-0.07	
	-10, 10	-0.21(0.03)	10.7(0.3)	3.3(0.7)	-0.06	
	-20, 10	-0.11(0.03)	11.9(0.5)	3.0(1.3)	-0.04	0.04
	-20, 0	-0.14(0.03)	11.6(0.4)	3.0(1.0)	-0.04	
	-20, -10	-0.11(0.02)	10.9(0.3)	2.4(0.6)	-0.04	0.16
	-20, -20	N				0.07
	-10, -20	-0.09(0.03)	10.1(0.6)	2.6(1.2)	-0.03	0.10
	0, -20	-0.16(0.02)	9.1(0.1)	1.2(0.9)	-0.13	0.18
	10, -20	-0.09(0.02)	10.0(0.3)	1.7(0.4)	-0.05	0.21
	20, -20	-0.12(0.03)	9.8(0.3)	2.4(0.4)	-0.05	0.21
	20, -10	-0.09(0.03)	9.2(0.4)	2.4(0.7)	-0.03	0.18
	20, 0	-0.08(0.02)	9.0(0.3)	1.6(0.8)	-0.05	0.10
	20, 10	-0.03(0.02)	10.8(0.8)	1.5(0.9)	-0.02	0.05
	20, 20	N				
	10, 20	N				0.03
	0, 20	-0.12(0.02)	9.9(0.2)	2.0(0.4)	-0.05	
	-10, 20	-0.14(0.03)	11.1(0.2)	1.8(0.8)	-0.07	
	-20, 20	-0.10(0.03)	12.0(0.4)	2.5(0.8)	-0.04	0.09
	-30, 20	N				0.10
	-30, 10	-0.07(0.03)	13.6(0.4)	1.4(0.6)	-0.05	0.06
	-30, 0	-0.10(0.02)	11.9(0.2)	2.3(0.5)	-0.04	
	-30, -10	-0.21(0.03)	11.8(0.3)	3.7(0.7)	-0.05	

Table B.3. continued.

Sources	Offset (arcmin)	Flux (K km s ⁻¹)	Velocity (km s ⁻¹)	Width (km s ⁻¹)	T _L (K)	T _C (K)
	-30, -20	-0.10(0.03)	8.5(0.4)	2.6(0.7)	-0.04	0.06
	-30, -30	-0.14(0.05)	9.2(0.5)	3.4(1.7)	-0.04	0.10
	-20, -30	-0.07(0.03)	9.8(0.4)	1.7(0.6)	-0.04	0.17
	-10, -30	-0.09(0.04)	9.5(0.9)	3.4(0.0)	-0.02	0.11
	0, -30	-0.22(0.03)	8.9(0.2)	2.6(0.4)	-0.08	0.18
	10, -30	-0.23(0.03)	9.6(0.1)	2.0(0.4)	-0.10	0.18
	20, -30	-0.11(0.03)	8.9(0.3)	2.2(0.5)	-0.05	0.23
	20, 30	-0.14(0.05)	9.6(0.6)	3.4(0.3)	-0.04	0.69
	10, 30	-0.19(0.04)	10.0(0.4)	4.2(0.3)	-0.04	
	0, 30	-0.08(0.02)	10.1(0.3)	1.7(0.7)	-0.04	0.25
	-10, 30	-0.13(0.02)	11.9(0.1)	2.1(0.4)	-0.06	0.45
	-20, 30	N				
	-30, 30	N				0.10
	-30, -40	-0.12(0.03)	11.8(0.3)	2.2(0.9)	-0.05	0.46
	-20, -40	-0.05(0.02)	12.4(0.5)	1.2(1.9)	-0.04	0.19
	-10, -40	-0.09(0.02)	8.4(0.4)	1.4(0.7)	-0.06	0.22
	0, -40	-0.24(0.03)	9.3(0.1)	2.3(0.3)	-0.10	0.20
	10, -40	-0.15(0.03)	9.9(0.2)	2.0(0.3)	-0.07	0.15
	20, -40	-0.11(0.04)	9.2(0.2)	1.7(1.4)	-0.06	0.28
	-30, -50	-0.19(0.03)	12.1(0.2)	2.2(0.4)	-0.08	0.23
	-20, -50	-0.04(0.02)	11.9(0.4)	1.2(1.6)	-0.03	0.46
	-10, -50	N				0.27
	0, -50	N				0.13
	10, -50	-0.07(0.03)	10.3(0.4)	1.5(1.0)	-0.05	0.42
	20, -50	N				0.25
S156	0, 0	-0.32(0.03)	-50.2(0.2)	3.8(0.5)	-0.08	0.69
	-10, 0	-0.09(0.02)	-49.0(0.3)	1.6(0.6)	-0.05	0.14
	-10, -10	-0.13(0.03)	-48.7(0.4)	4.3(1.1)	-0.03	0.15
	0, -10	-0.33(0.04)	-50.2(0.2)	2.8(0.3)	-0.11	0.24
	10, -10	N				0.07
	10, 0	N				0.28
	10, 10	-0.09(0.03)	-50.1(0.2)	2.9(0.5)	-0.03	0.13
	0, 10	-0.21(0.03)	-50.2(0.2)	2.4(0.4)	-0.08	0.08
	-10, 10	-0.08(0.02)	-49.0(0.3)	2.4(0.6)	-0.03	0.14
	-20, 10	-0.05(0.02)	-45.0(0.4)	1.6(1.7)	-0.03	0.16
	-20, 0	-0.04(0.01)	-44.9(0.2)	1.2(1.6)	-0.03	0.11
	-20, -10	N				0.07
	-20, -20	-0.04(0.01)	-48.7(0.2)	1.2(1.9)	-0.03	
	-10, -20	-0.12(0.04)	-49.5(0.6)	3.1(1.5)	-0.04	
	0, -20	-0.20(0.03)	-49.4(0.2)	2.8(0.5)	-0.07	
	10, -20	-0.09(0.03)	-50.6(0.5)	2.7(1.0)	-0.03	0.12
	10, 20	-0.08(0.03)	-50.4(0.4)	2.0(0.6)	-0.04	0.37
	0, 20	-0.07(0.02)	-49.1(0.3)	1.8(0.6)	-0.03	0.57
	-10, 20	-0.13(0.03)	-50.3(0.4)	3.3(0.9)	-0.04	0.18
	-20, 20	-0.10(0.04)	-51.1(0.7)	3.5(1.4)	-0.03	0.23
	-30, 20	N				0.38
	-30, 10	-0.08(0.02)	-50.2(0.4)	2.1(0.7)	-0.04	0.16
	-30, 0	N				0.22
	-30, -10	-0.09(0.04)	-46.8(0.9)	3.5(1.6)	-0.02	0.09
	-30, -20	N				0.41
	-30, -30	-0.08(0.03)	-54.3(0.4)	1.5(0.8)	-0.05	0.34
	-20, -30	N				0.30
	-10, -30	N				0.26
	0, -30	N				0.16
	10, -30	N				0.36
	10, 30	N				0.16
	0, 30	N				0.13
	-10, 30	N				0.14
	-20, 30	N				0.08
	-30, 30	N				

Table B.3. continued.

Sources	Offset (arcmin)	Flux (K km s ⁻¹)	Velocity (km s ⁻¹)	Width (km s ⁻¹)	T _L (K)	T _C (K)	
DR17/L906	0, 0	-0.37(0.05)	7.0(0.2)	3.9(0.6)	-0.09	1.64	
	-10, 0	-0.11(0.02)	5.8(0.3)	3.0(0.6)	-0.03	0.31	
	-10, -10	-0.09(0.03)	7.7(0.5)	3.2(1.0)	-0.03	0.38	
	0, -10	-0.06(0.03)	6.9(0.3)	1.5(0.8)	-0.04	0.50	
			-0.09(0.03)	9.8(0.5)	2.6(1.0)	-0.03	
	10, -10	-0.10(0.02)	7.1(0.2)	1.4(0.8)	-0.06	0.58	
			-0.26(0.03)	15.4(0.2)	3.1(0.4)	-0.08	
	10, 0	-0.14(0.02)	6.5(0.2)	2.4(0.5)	-0.05	1.08	
	10, 10	-0.07(0.01)	6.6(0.2)	1.5(0.8)	-0.04	0.83	
	0, 10	-0.23(0.03)	6.2(0.3)	3.7(0.5)	-0.06	1.61	
			-0.05(0.02)	14.7(0.4)	1.7(0.6)	-0.03	
	-10, 10	-0.07(0.02)	6.8(0.3)	2.2(0.6)	-0.03	0.26	
	-10, -20	-0.06(0.03)	5.9(0.5)	1.6(1.3)	-0.04	0.43	
	0, -20	-0.06(0.02)	6.4(0.3)	1.9(0.5)	-0.03	0.39	
			-0.05(0.02)	10.7(0.4)	1.7(0.8)	-0.03	
	10, -20	-0.12(0.02)	6.5(0.2)	2.5(0.5)	-0.04	0.44	
	20, -20	-0.22(0.03)	4.6(0.2)	2.4(0.5)	-0.08	0.52	
			-0.07(0.02)	14.0(0.1)	1.2(1.5)	-0.06	
	20, -10	-0.05(0.02)	4.6(0.4)	2.1(0.8)	-0.02	0.63	
			-0.11(0.02)	15.8(0.2)	2.7(0.6)	-0.04	
	20, 0		N				0.57
	20, 10		N				0.53
	20, 20		N				0.24
	10, 20	-0.11(0.03)	5.7(0.6)	3.9(1.0)	-0.03	0.49	
	0, 20	-0.08(0.04)	9.7(0.4)	2.0(1.2)	-0.04	0.54	
	-10, 20	-0.09(0.04)	7.5(0.7)	3.0(1.2)	-0.03	0.16	
	-10, -30		N				0.35
	0, -30	-0.05(0.02)	5.4(0.2)	1.2(0.8)	-0.04	0.36	
	10, -30	-0.09(0.02)	7.4(0.2)	1.7(0.3)	-0.05	0.49	
	20, -30	-0.25(0.01)	6.6(0.3)	4.6(0.5)	-0.05	0.51	
			-0.05(0.02)	14.0(0.1)	1.2(1.6)	-0.04	
	M17/M18	0, 0	-0.17(0.04)	16.6(0.1)	1.7(1.1)	-0.10	31.1
		-0.36(0.04)	22.2(0.1)	2.1(0.3)	-0.16		
		-0.08(0.04)	38.1(0.6)	2.1(1.6)	-0.03		
-10, 0		-0.49(0.06)	15.0(1.2)	4.3(1.2)	-0.11	13.9	
		-0.43(0.06)	19.2(1.2)	3.2(1.2)	-0.13		
		-0.41(0.06)	22.4(1.2)	1.3(1.2)	-0.29		
-10, -10		-0.32(0.04)	18.7(0.4)	5.0(0.6)	-0.06	0.95	
		-0.06(0.03)	26.2(0.2)	1.2(1.7)	-0.04		
0, -10		-0.10(0.05)	18.4(0.5)	2.5(1.2)	-0.04	6.58	
		-0.10(0.03)	21.2(0.1)	1.2(1.6)	-0.08		
10, -10			N			1.35	
10, 0			N			2.37	
10, 10		-0.05(0.05)	20.9(1.2)	1.2(1.6)	-0.04	1.81	
		-0.06(0.05)	22.7(0.5)	1.2(1.0)	-0.05		
0, 10		-0.24(0.05)	17.8(0.4)	3.8(0.9)	-0.06	5.95	
		-0.13(0.04)	22.3(0.4)	2.1(0.7)	-0.05		
-10, 10		-0.54(0.06)	17.5(0.2)	3.8(0.6)	-0.13	4.99	
		-0.10(0.04)	21.9(0.4)	1.5(0.5)	-0.06		
-20, 10		-0.06(0.02)	39.3(0.2)	1.2(1.3)	-0.05	0.60	
-20, 0		-0.10(0.02)	30.2(0.2)	1.7(0.4)	-0.06	1.05	
-20, -10		-0.07(0.04)	18.1(1.1)	2.9(1.4)	-0.02	0.55	
-20, -20		-0.31(0.04)	17.6(0.2)	3.3(0.5)	-0.09	0.59	
			-0.07(0.03)	28.4(0.5)	1.9(0.9)	-0.03	
			-0.08(0.04)	37.0(0.5)	2.1(1.5)	-0.04	
-10, -20		-0.07(0.02)	18.1(0.3)	1.7(0.5)	-0.04	0.25	
		-0.04(0.02)	26.0(0.2)	1.2(1.3)	-0.03		
0, -20		-0.25(0.03)	17.7(0.1)	2.2(0.3)	-0.11	0.38	
		-0.05(0.02)	32.2(0.2)	1.2(1.5)	-0.04		
10, -20	-0.06(0.02)	19.2(0.3)	1.5(0.7)	-0.04	0.66		

Table B.3. continued.

Sources	Offset (arcmin)	Flux (K km s ⁻¹)	Velocity (km s ⁻¹)	Width (km s ⁻¹)	T _L (K)	T _C (K)
	20, -20	-0.03(0.03)	21.8(0.8)	1.2(1.6)	-0.02	0.39
		-0.13(0.06)	37.8(1.3)	5.0(2.0)	-0.02	
	20, -10	-0.06(0.04)	15.5(0.7)	2.2(1.4)	-0.03	0.56
	20, 0	-0.03(0.02)	35.4(0.4)	1.2(1.1)	-0.02	0.13
	20, 10	N				0.11
	20, 20	N				0.10
	10, 20	-0.09(0.03)	21.5(0.6)	3.6(1.0)	-0.02	0.28
	0, 20	-0.16(0.04)	19.9(0.8)	5.9(1.7)	-0.03	0.56
	-10, 20	-0.07(0.02)	20.0(0.1)	1.2(1.4)	-0.05	0.55
	-20, 20	-0.11(0.03)	21.3(0.1)	1.2(1.3)	-0.09	0.08
		-0.05(0.02)	29.4(0.4)	1.2(0.7)	-0.04	
	-30, 20	-0.07(0.03)	29.2(0.6)	2.5(0.7)	-0.03	0.07
	-30, 10	-0.04(0.03)	28.6(0.3)	1.2(1.5)	-0.03	0.16
		-0.05(0.03)	39.3(0.3)	1.2(1.4)	-0.04	
	-30, 0	-0.05(0.02)	22.0(0.3)	1.2(0.3)	-0.04	0.26
	-30, -10	-0.06(0.02)	23.7(0.1)	1.2(1.5)	-0.04	0.29
		-0.07(0.02)	27.3(0.2)	1.8(1.0)	-0.04	
		-0.16(0.03)	39.1(0.2)	2.8(0.5)	-0.05	
	-30, -20	-0.06(0.02)	16.9(0.2)	1.2(0.8)	-0.05	0.24
		-0.15(0.03)	20.7(0.3)	3.6(0.8)	-0.04	
		-0.04(0.02)	41.8(0.2)	1.2(1.9)	-0.03	
	-30, -30	-0.72(0.06)	18.2(0.2)	4.0(0.4)	-0.17	0.21
		-0.10(0.05)	32.6(0.9)	2.9(1.7)	-0.03	
	-20, -30	-0.74(0.05)	18.6(0.1)	3.9(0.4)	-0.18	0.68
		-0.06(0.03)	34.9(0.6)	1.8(1.1)	-0.03	
	-10, -30	-0.44(0.04)	18.7(0.1)	3.1(0.3)	-0.13	
		-0.11(0.04)	35.4(0.6)	3.1(1.0)	-0.03	
	0, -30	-0.24(0.06)	16.8(0.6)	4.5(1.3)	-0.05	0.16
		-0.05(0.04)	34.2(1.2)	1.2(1.5)	-0.04	
	10, -30	-0.08(0.04)	19.6(0.3)	1.7(0.7)	-0.05	0.23
		-0.07(0.04)	34.4(0.4)	1.9(1.5)	-0.04	
	20, -30	-0.05(0.03)	37.2(1.0)	1.6(1.5)	-0.03	0.10
	20, 30	N				0.08
	10, 30	-0.09(0.05)	28.9(0.9)	3.0(1.1)	-0.03	
	0, 30	N				0.18
	-10, 30	-0.04(0.03)	25.6(0.8)	1.2(1.4)	-0.03	0.06
	-20, 30	-0.04(0.04)	23.9(0.6)	1.2(1.4)	-0.03	0.17
	-30, 30	-0.08(0.03)	23.4(0.3)	1.2(1.1)	-0.06	0.26
		-0.11(0.04)	28.1(0.4)	1.6(0.6)	-0.06	
		-0.06(0.04)	38.3(0.3)	1.2(1.2)	-0.05	
	-40, 30	-0.14(0.05)	26.9(0.4)	2.0(0.7)	-0.07	0.23
	-40, 20	-0.16(0.07)	27.5(1.3)	4.4(2.0)	-0.03	0.17
	-40, 10	-0.71(0.06)	25.4(0.2)	4.3(0.3)	-0.16	
	-40, 0	-0.11(0.04)	26.3(0.2)	1.2(1.9)	-0.09	
		-0.26(0.04)	36.9(0.1)	1.2(1.6)	-0.21	
	-40, -10	-0.37(0.06)	37.8(0.3)	3.3(0.6)	-0.10	0.17
	-40, -20	-0.10(0.04)	18.9(0.2)	1.2(1.9)	-0.08	0.30
		-0.08(0.05)	23.9(0.9)	2.7(1.3)	-0.03	
		-0.22(0.08)	35.3(0.8)	4.0(1.8)	-0.05	
	-40, -30	-0.11(0.04)	34.0(0.6)	3.2(1.0)	-0.03	0.55
	-40, -40	-0.62(0.07)	18.3(0.2)	3.1(0.4)	-0.19	0.67
		-0.12(0.06)	32.6(1.0)	3.5(1.5)	-0.03	
	-30, -40	-1.11(0.03)	18.5(0.1)	2.7(0.1)	-0.39	0.72
		-0.08(0.04)	36.8(0.3)	1.2(1.2)	-0.06	
	-20, -40	-0.88(0.06)	18.7(0.1)	3.4(0.2)	-0.24	
		-0.05(0.03)	36.5(0.6)	1.2(1.5)	-0.04	
	-10, -40	-0.22(0.05)	18.3(0.4)	3.5(1.1)	-0.06	0.15
		-0.09(0.04)	37.1(0.7)	2.8(1.6)	-0.03	
	0, -40	-0.06(0.03)	18.6(0.6)	1.9(1.5)	-0.03	
	10, -40	-0.23(0.06)	26.2(0.1)	1.2(1.8)	-0.18	

Table B.3. continued.

Sources	Offset (arcmin)	Flux (K km s ⁻¹)	Velocity (km s ⁻¹)	Width (km s ⁻¹)	T _L (K)	T _C (K)
	20, -40	N				0.05

Notes. Parameters listed concern the simultaneously observed H₂CO absorption line. "N" indicates that the corresponding spectra could not be detected or the line peak intensity is less than 0.02 K.

Table B.4. Parameters of the ¹²CO (1–0) and ¹³CO (1–0) emission lines.

Sources	¹² CO					¹³ CO			
	Offset (arcmin)	Flux (K km s ⁻¹)	Velocity (km s ⁻¹)	Width (km s ⁻¹)	T _L (K)	Flux (K km s ⁻¹)	Velocity (km s ⁻¹)	Width (km s ⁻¹)	T _L (K)
MON R2	0, 0	35.76(0.97)	10.2	3.9	8.60	7.53(0.07)	10.3	2.2	3.26
	-10, 0	24.62(0.12)	10.7	3.9	6.01	4.73(0.05)	10.7	2.9	1.53
	-10, -10	21.28(0.11)	10.7	2.5	8.00	4.29(0.04)	10.6	2.1	1.90
	0, -10	13.78(0.10)	10.7	1.8	7.37	2.57(0.03)	10.6	1.4	1.71
	10, -10	6.60(0.07)	10.0	1.8	3.48	1.36(0.03)	10.0	1.3	0.99
	10, 0	11.76(0.08)	9.5	2.0	5.50	2.82(0.03)	9.5	1.6	1.62
	10, 10	12.56(0.11)	9.4	2.1	5.64	1.94(0.04)	9.3	1.5	1.23
	0, 10	9.81(0.11)	10.3	2.5	3.65	1.92(0.06)	10.4	1.6	1.10
	-10, 10	14.70(0.31)	10.7	2.5	5.44	3.17(0.04)	10.8	1.6	1.84
	-20, 10	18.81(0.11)	12.0	3.6	4.97	3.46(0.04)	12.0	2.7	1.20
	-20, 0	21.83(0.10)	11.6	3.5	5.81	3.76(0.04)	11.7	2.9	1.20
	-20, -10	16.87(0.10)	11.1	2.8	5.58	2.72(0.04)	11.1	2.0	1.28
	-20, -20	11.46(0.11)	11.2	3.0	3.65	1.66(0.03)	11.2	2.1	0.73
	-10, -20	13.90(0.15)	10.3	2.9	4.52	2.57(0.04)	10.1	2.2	1.13
	0, -20	13.70(0.08)	9.9	2.7	4.81	2.67(0.04)	10.0	2.1	1.22
	10, -20	8.33(0.07)	10.4	2.1	3.81	1.56(0.03)	10.4	1.3	1.12
	20, -20	7.06(0.05)	10.1	2.3	2.86	1.16(0.04)	9.9	1.4	0.79
	20, -10	3.74(0.09)	9.4	1.4	2.56	0.62(0.03)	9.4	0.9	0.62
	20, 0	7.38(0.08)	9.0	1.6	4.33	1.51(0.03)	9.0	1.3	1.11
	20, 10	7.09(0.10)	9.6	1.9	3.59	0.92(0.05)	9.4	1.4	0.61
	20, 20	3.02(0.08)	9.6	1.3	2.13	0.44(0.05)	9.7	2.0	0.21
		8.77(0.09)	12.5	2.0	4.17	1.53(0.04)	12.6	1.0	1.39
	10, 20	6.55(0.09)	10.0	1.5	4.08	1.02(0.03)	10.0	1.1	0.89
		6.38(0.10)	12.5	2.1	2.91	0.72(0.04)	12.6	1.3	0.51
	0, 20	8.02(0.15)	10.7	1.7	4.38	1.34(0.08)	10.5	1.0	1.23
	-10, 20	16.05(0.13)	11.2	3.0	5.00	3.54(0.04)	11.4	2.7	1.24
	-20, 20	16.10(0.10)	12.4	3.2	4.70	2.99(0.04)	12.5	2.1	1.33
	-30, 20	13.55(0.14)	12.8	4.6	2.76	1.36(0.04)	13.1	2.2	0.57
	-30, 10	14.61(0.15)	11.5	4.3	3.17	1.67(0.05)	12.1	3.2	0.49
	-30, 0	14.82(0.12)	11.0	3.4	4.06	1.90(0.05)	11.0	2.5	0.71
	-30, -10	15.27(0.11)	11.0	3.4	4.17	2.16(0.05)	11.0	2.2	0.93
	-30, -20	12.19(0.12)	10.6	3.6	3.17	1.79(0.05)	10.7	2.1	0.81
	-30, -30	12.44(0.23)	10.8	4.6	2.57	1.06(0.06)	11.1	2.6	0.39
	-20, -30	11.82(0.20)	11.3	3.6	3.13	1.26(0.04)	11.3	2.2	0.55
	-10, -30	11.83(1.69)	9.8	3.0	3.75	1.70(0.05)	10.0	2.3	0.71
		5.35(1.67)	13.6	3.1	1.61	0.56(0.04)	13.7	1.5	0.36
	0, -30	17.31(0.11)	9.7	3.6	4.49	3.15(0.06)	10.0	2.8	1.05
	10, -30	11.57(0.10)	10.1	3.0	3.63	2.40(0.04)	10.0	1.8	1.22
	20, -30	3.80(0.09)	9.6	1.9	1.89	0.51(0.03)	9.6	1.2	0.41
	20, 30	8.08(0.08)	12.6	1.7	4.50	0.73(0.04)	9.6	1.1	0.64
		4.43(0.06)	9.7	1.2	3.51	1.06(0.04)	12.7	1.2	0.81
	10, 30	5.48(0.07)	10.2	1.3	3.94	1.35(0.04)	10.2	1.2	1.04
		8.44(0.09)	12.6	1.8	4.45	1.07(0.03)	12.7	1.1	0.93
	0, 30	5.52(0.38)	10.2	1.5	3.41	1.64(0.04)	10.2	1.1	1.36
		5.57(0.42)	12.1	3.8	1.38	0.62(0.06)	13.2	2.1	0.28
	-10, 30	9.47(0.11)	11.9	3.4	2.65	1.86(0.04)	12.4	1.8	1.00
	-20, 30	13.91(0.12)	12.5	3.3	4.01	2.03(0.04)	12.6	2.0	0.94
	-30, 30	11.93(0.13)	12.7	4.2	2.66	1.23(0.04)	12.9	2.3	0.51
	-30, -40	11.75(0.17)	11.8	4.2	2.61	1.37(0.06)	12.1	2.4	0.53
	-20, -40	10.87(0.14)	11.7	3.5	2.91	1.43(0.05)	11.9	2.0	0.67

Table B.4. continued.

Sources	^{12}CO					^{13}CO			
	Offset (arcmin)	Flux (K km s $^{-1}$)	Velocity (km s $^{-1}$)	Width (km s $^{-1}$)	T_L (K)	Flux (K km s $^{-1}$)	Velocity (km s $^{-1}$)	Width (km s $^{-1}$)	T_L (K)
S156	-10, -40	11.04(0.15)	9.7	3.8	2.74	1.42(0.15)	8.9	2.5	0.54
		3.93(0.14)	13.6	2.2	1.70	0.85(0.17)	13.0	4.2	0.19
	0, -40	11.35(0.10)	9.9	2.9	3.70	3.02(0.05)	10.0	2.2	1.30
		2.52(0.09)	13.5	1.7	1.39	0.21(0.03)	13.5	1.1	0.18
	10, -40	9.62(0.09)	10.3	2.9	3.09	2.32(0.03)	10.3	1.8	1.21
	20, -40	6.60(0.08)	9.7	2.6	2.38	1.30(0.04)	10.0	2.1	0.59
	-30, -50	13.69(0.20)	11.6	4.0	3.23	2.59(0.06)	12.1	2.2	1.10
	-20, -50	12.05(0.19)	11.7	4.4	2.59	1.59(0.06)	12.3	2.8	0.54
	-10, -50	7.67(0.67)	10.0	3.6	2.02	1.29(0.06)	9.5	2.6	0.46
		5.25(0.67)	13.5	3.0	1.64	0.82(0.06)	13.2	1.9	0.41
	0, -50	6.14(0.12)	10.2	2.4	2.40	1.03(0.04)	10.3	1.5	0.65
		5.52(0.12)	13.5	2.7	1.95	0.75(0.04)	13.5	1.5	0.48
	10, -50	9.02(0.07)	11.2	3.9	2.17	1.26(0.02)	11.0	2.5	0.48
	20, -50	8.19(0.07)	10.5	3.5	2.22	0.89(0.04)	10.5	1.5	0.55
	0, 0	40.10(0.15)	-52.2	5.1	7.44	8.13(0.05)	-52.1	3.4	2.24
	-10, 0	16.45(0.11)	-50.7	4.9	3.16	2.01(0.04)	-50.8	3.1	0.61
	-10, -10	15.90(0.14)	-50.2	5.6	2.68	2.39(0.04)	-50.4	4.1	0.56
	0, -10	28.97(0.21)	-51.7	5.1	5.31	5.86(0.04)	-51.8	3.1	1.75
	10, -10	24.15(0.36)	-50.8	6.1	3.73	2.59(0.08)	-50.5	3.9	0.63
	10, 0	21.29(0.72)	-52.9	3.7	5.40	3.84(0.11)	-52.7	3.6	1.00
		12.68(0.75)	-48.7	6.8	1.74				
	10, 10	17.93(0.34)	-53.1	3.1	5.47	3.30(0.12)	-53	2.4	1.30
		7.63(0.35)	-49.2	3.5	2.04				
	0, 10	34.76(0.10)	-51.1	4.8	6.78	6.89(0.05)	-51.2	3.7	1.75
	-10, 10	15.34(0.12)	-50.3	5.1	2.82	1.69(0.05)	-50.5	3.3	0.48
	-20, 10	3.24(0.12)	-51.6	5.0	0.61				
	-20, 0	4.26(0.12)	-50.3	7.4	0.54				
	-20, -10	6.93(0.16)	-47.7	4.1	1.59	1.03(0.04)	-47.7	3.7	0.26
	-20, -20	2.70(0.26)	-51.9	4.4	0.58	0.68(0.06)	-51.1	9.8	0.07
		2.10(0.22)	-47.5	2.9	0.69				
	-10, -20	18.41(0.18)	-49.4	6.8	2.54	2.86(0.04)	-49.7	5.9	0.46
	0, -20	18.92(0.22)	-51.0	5.2	3.40	2.91(0.05)	-51.1	3.2	0.85
		4.73(0.18)	-45.8	3.7	1.20				
	10, -20	17.19(0.20)	-50.6	4.2	3.87	1.99(0.07)	-50.6	2.6	0.71
		6.68(0.17)	-45.7	3.0	2.07				
	10, 20	3.18(0.20)	-53.1	2.5	1.20	0.35(0.08)	-53.0	0.9	0.35
		2.93(0.19)	-50.3	1.9	1.45				
	0, 20	5.53(0.09)	-51.8	4.3	1.21	0.91(0.04)	-51.2	3.4	0.25
	-10, 20	15.50(0.11)	-51.1	5.6	2.61	2.08(0.04)	-51.3	5.0	0.39
	-20, 20	7.82(0.09)	-53.2	3.3	2.22	1.01(0.04)	-53.2	2.4	0.39
-30, 20	6.05(0.15)	-53.5	5.0	1.15	0.43(0.12)	-54.0	3.0	0.14	
-30, 10	3.05(0.19)	-51.9	4.8	0.60					
-30, 0	4.97(0.24)	-51.2	6.9	0.68					
-30, -10	1.32(0.14)	-47.6	1.5	0.81					
-30, -20	2.53(0.22)	-50.0	7.1	0.33					
-30, -30	2.07(0.22)	-56.2	4.2	0.46					
-20, -30	2.86(0.17)	-50.5	7.8	0.34					
-10, -30	3.42(0.16)	-49.2	5.7	0.56					
0, -30	7.22(0.16)	-49.3	7.8	0.87	0.51(0.05)	-50.2	5.8	0.08	
10, -30	11.92(0.20)	-48.8	6.4	1.75	0.80(0.07)	-49.5	3.4	0.22	
10, 30	4.28(0.47)	-50.5	6.7	0.60					
0, 30	1.67(0.14)	-53.6	3.0	0.53					
-10, 30	7.54(0.20)	-53.5	4.1	1.71	0.72(0.06)	-53.3	2.4	0.28	
-20, 30	8.48(0.17)	-53.0	3.9	2.02	0.75(0.06)	-52.4	2.3	0.31	
-30, 30	8.19(0.32)	-54.5	2.9	2.63	1.07(0.18)	-54.4	2.0	0.51	
DR17/L906	0, 0	9.67(0.10)	4.9	3.7	2.45	3.03(0.12)	6.0	6.0	0.48
		4.31(0.10)	14.9	3.2	1.25	0.49(0.07)	15.3	2.4	0.20
		1.94(0.10)	-2.8	4.6	0.40				
		1.16(0.10)	-0.6	2.3	0.48				

Table B.4. continued.

Sources	Offset (arcmin)	¹² CO				¹³ CO			
		Flux (K km s ⁻¹)	Velocity (km s ⁻¹)	Width (km s ⁻¹)	T _L (K)	Flux (K km s ⁻¹)	Velocity (km s ⁻¹)	Width (km s ⁻¹)	T _L (K)
		6.59(0.10)	9.5	4.2	1.47				
	-10, 0	6.54(0.15)	-1.3	3.2	1.94	0.82(0.07)	-1.0	2.5	0.31
		5.58(0.13)	4.8	3.2	1.63	0.60(0.07)	4.8	2.1	0.28
		1.19(0.11)	-5.5	1.9	0.58				
	-10, -10	8.27(0.27)	5.9	4.3	1.80	1.50(0.20)	6.3	5.8	0.25
		0.72(0.16)	-4.7	1.5	0.47				
		3.36(0.18)	10.0	1.6	1.99				
	0, -10	8.57(0.16)	5.3	3.3	2.41	1.28(0.09)	5.3	2.8	0.43
		3.63(0.33)	9.3	2.0	1.72	1.12(0.08)	9.1	2.0	0.53
		3.63(0.15)	-3.8	3.7	0.92				
		6.29(0.37)	12.3	4.1	1.43				
	10, -10	9.55(0.20)	5.0	3.7	2.46	1.46(0.08)	5.4	3.5	0.39
		35.67(0.23)	14.3	5.2	6.45	6.91(0.08)	14.3	4.1	1.59
	10, 0	9.66(0.43)	0.5	6.2	1.46	0.98(0.09)	0.1	3.0	0.31
		4.97(0.94)	4.6	2.4	1.97	1.48(0.09)	5.0	2.6	0.54
		6.41(0.18)	13.9	3.6	1.68	0.88(0.08)	14.1	3.1	0.27
		4.61(0.91)	7.0	3.8	1.15				
	10, 10	6.54(0.19)	4.3	4.4	1.39	1.60(0.08)	4.4	4.5	0.33
		3.75(0.37)	-1.2	6.4	0.55				
		3.24(0.22)	7.8	10.8	0.28				
	0, 10	2.57(0.64)	4.0	3.0	0.82	0.37(0.06)	4.8	1.7	0.21
		14.81(0.44)	9.6	7.8	1.79	2.36(0.13)	8.0	10.0	0.22
		3.69(0.84)	0.7	7.2	0.48				
	-10, 10	5.55(0.13)	-2.8	4.3	1.21	0.55(0.05)	-2.8	2.7	0.19
		4.53(0.10)	4.8	2.5	1.70	0.69(0.04)	5.1	1.8	0.35
	-10, -20	3.53(0.13)	9.9	1.8	1.81	0.58(0.09)	10.1	1.5	0.37
		2.85(0.17)	5.0	3.4	0.79				
	0, -20	6.57(0.29)	5.1	3.7	1.69	1.06(0.08)	5.7	3.8	0.26
		7.17(0.28)	9.4	3.0	2.26	1.31(0.06)	9.5	1.8	0.69
	10, -20	11.29(0.36)	5.4	4.4	2.40	1.96(0.06)	6.0	2.7	0.69
		12.63(0.34)	13.8	4.4	2.69	2.46(0.08)	14.1	4.8	0.49
	20, -20	6.11(1.11)	3.4	3.0	1.94	2.88(0.09)	3.5	5.0	0.54
		20.59(1.14)	13.2	4.6	4.18	3.40(0.08)	12.5	5.0	0.64
		3.24(0.32)	-0.5	1.9	1.61				
		8.62(1.33)	7.2	6.0	1.34				
	20, -10	2.55(0.29)	-0.7	1.8	1.32	0.63(0.06)	-0.9	2.2	0.27
		3.39(0.37)	3.9	3.3	0.97	0.68(0.07)	4.0	2.7	0.24
		19.38(0.41)	15.1	4.2	4.37	3.40(0.08)	15.2	3.5	0.90
	20, 0	11.98(0.26)	-0.3	6.3	1.79	1.77(0.10)	-0.1	6.1	0.27
		1.97(0.17)	-4.7	2.2	0.86				
	20, 10	7.11(0.18)	2.0	3.9	1.72	1.31(0.06)	2.2	3.4	0.36
		2.14(0.09)	-4.8	3.2	0.62				
		4.66(0.21)	9.3	7.1	0.62				
	20, 20	15.32(0.16)	3.4	7.6	1.89	2.59(0.08)	3.3	4.6	0.53
	10, 20	12.84(0.17)	3.8	4.0	3.01	2.28(0.07)	3.5	2.6	0.82
		1.06(0.07)	-5.1	2.4	0.42				
		1.91(0.19)	10.1	5.2	0.35				
	0, 20	3.27(0.12)	-4.6	2.5	1.24	0.39(0.05)	-4.3	1.4	0.26
		4.63(0.15)	4.4	3.4	1.30	0.77(0.06)	4.2	2.7	0.27
		8.78(0.16)	11.1	4.4	1.88	1.15(0.06)	11.7	2.7	0.4
	-10, 20	7.05(0.10)	-4.1	3.4	1.95	0.77(0.06)	-4.1	1.9	0.38
		3.87(0.12)	3.2	5.4	0.67				
		1.40(0.06)	9.6	2.3	0.58				
	-10, -30	6.78(0.41)	3.9	3.3	1.94	0.82(0.17)	3.5	3.0	0.26
	0, -30	10.12(0.40)	4.3	8.4	1.13	1.32(0.12)	4.7	7.6	0.16
	10, -30	5.38(0.25)	-2.6	2.9	1.74	0.80(0.08)	-2.7	2.6	0.29
		8.00(0.40)	5.9	3.6	2.11	1.85(0.09)	6.3	3.1	0.56
		4.42(0.44)	11.9	5.1	0.82				
	20, -30	18.16(0.84)	6.8	6.4	2.65	3.38(0.15)	6.8	6.3	0.51

Table B.4. continued.

Sources	Offset (arcmin)	¹² CO				¹³ CO			
		Flux (K km s ⁻¹)	Velocity (km s ⁻¹)	Width (km s ⁻¹)	T _L (K)	Flux (K km s ⁻¹)	Velocity (km s ⁻¹)	Width (km s ⁻¹)	T _L (K)
M17/M18	0, 0	15.39(0.75)	13.5	3.9	3.68	2.04(0.11)	13.5	3.0	0.63
		2.60(0.41)	-2.0	3.9	0.63				
	52.23(0.23)	20.7	7.9	6.20	6.83(0.11)	20.6	7.1	0.91	
	15.54(0.25)	35.6	10.3	1.42	3.73(0.13)	34.7	10.2	0.34	
	4.98(0.21)	55.1	7.6	0.61	1.12(0.11)	55.8	9.0	0.12	
	2.38(0.17)	79.5	5.8	0.39					
	-10, 0	67.67(0.40)	19.8	7.5	8.46	10.90(0.15)	20.1	6.2	1.65
		23.19(0.49)	31.5	11.5	1.89	6.76(0.18)	31.3	9.0	0.71
	-10, -10	6.62(0.19)	43.3	4.4	1.41	2.12(0.14)	43.5	5.9	0.34
		2.53(0.14)	76.9	4.8	0.50				
		42.94(0.22)	19.9	6.3	6.42	6.35(0.21)	19.8	4.8	1.24
		14.14(0.22)	30.9	9.3	1.42	4.32(0.39)	28.7	10.2	0.40
	0, -10	7.00(0.22)	38.3	5.0	1.31	1.37(0.23)	38.1	5.2	0.25
		5.10(0.22)	44.8	3.7	1.31	1.09(0.08)	44.6	2.7	0.37
		20.01(0.24)	21.1	6.2	3.06	2.11(0.22)	21.4	5.7	0.35
		8.28(0.34)	30.3	7.3	1.07	1.93(0.38)	28.7	6.1	0.29
	10, -10	8.19(0.23)	37.9	4.3	1.77	1.45(0.10)	38.1	2.8	0.48
		6.38(0.18)	56.3	8.8	0.68				
		5.13(0.07)	22.3	5.7	0.85	0.32(0.09)	22.0	3.8	0.08
		9.91(0.07)	30.9	9.5	0.98	2.46(0.18)	30.9	11.4	0.20
	10, 0	3.56(0.07)	38.3	3.2	1.06	0.45(0.08)	38.0	2.6	0.17
		6.59(0.07)	57.4	6.5	0.96	0.76(0.07)	57.2	6.4	0.11
		4.28(0.07)	77.1	5.5	0.73				
		0.88(0.17)	16.1	2.1	0.40	0.27(0.05)	15.8	1.2	0.21
	10, 10	11.05(0.54)	26.0	14.0	0.74				
		8.55(0.39)	36.0	5.2	1.55	1.16(0.08)	35.6	3.4	0.32
		8.06(0.18)	58.4	5.0	1.51	0.81(0.08)	58.8	2.9	0.26
		7.81(1.03)	21.4	11.6	0.63				
	0, 10	5.16(1.36)	31.3	6.7	0.72	0.96(0.16)	31.3	7.9	0.11
		5.12(0.57)	36.1	3.7	1.29	0.57(0.12)	35.8	2.5	0.22
		8.23(0.29)	56.4	5.3	1.45	0.97(0.08)	56.3	4.8	0.19
		7.55(0.22)	-0.6	10.3	0.69				
	-10, 10	40.20(0.22)	19.6	5.2	7.25	5.27(0.10)	19.8	4.0	1.24
		18.27(0.22)	34.9	15.2	1.13	1.70(0.14)	34.0	5.7	0.28
		1.15(0.22)	45.2	2.1	0.50				
		5.93(0.22)	55.5	3.9	1.44	0.89(0.09)	55.7	3.8	0.22
	-20, 10	8.55(0.32)	1.7	10.8	0.74				
		33.07(0.42)	19.5	4.6	6.75	5.41(0.09)	19.6	3.6	1.41
		22.26(0.75)	31.4	15.6	1.34	2.53(0.41)	32.9	6.5	0.37
		7.01(0.35)	43.6	4.7	1.4	2.59(0.25)	43.8	9.8	0.25
-20, 0	24.43(0.40)	28.9	12.1	1.9	0.87(0.11)	30.1	3.1	0.27	
	11.75(0.35)	41.6	7.7	1.43	5.16(0.22)	35.7	22.0	0.22	
	40.79(0.13)	28.9	15.1	2.54	0.81(0.11)	26.1	3.0	0.26	
	6.74(0.13)	41.3	6.6	0.97	6.78(0.15)	28.9	9.1	0.70	
-20, -10	3.19(0.13)	61.3	3.6	0.84	0.44(0.09)	39.3	3.3	0.12	
	6.83(0.13)	75.7	10.8	0.59	0.41(0.06)	61.3	1.4	0.27	
	27.65(0.23)	19.9	5.9	4.43	2.65(0.18)	19.1	4.2	0.60	
	37.08(0.23)	28.3	12.5	2.79	6.90(0.12)	28.3	6.5	1.00	
-20, -20	16.46(0.23)	41.1	7.3	2.11	3.11(0.11)	39.4	6.9	0.43	
	1.18(0.23)	60.0	2.5	0.45	0.39(0.05)	60.2	1.8	0.20	
	1.64(0.23)	75.2	6.0	0.26					
	43.25(0.23)	19.2	7.2	5.62	8.32(0.15)	18.7	3.7	2.13	
-10, -20	13.85(0.23)	28.4	6.7	1.94	5.11(0.15)	26.5	8.6	0.56	
	20.69(0.23)	36.7	6.9	2.84	3.90(0.15)	36.5	5.6	0.66	
	5.50(0.23)	44.8	5.3	0.97					
	1.41(0.23)	59.8	2.4	0.55					
-10, -20	7.89(0.11)	20.0	3.8	1.93	0.88(0.07)	19.6	2.5	0.33	
	13.04(0.11)	28.4	12.1	1.01	2.16(0.19)	27.0	8.1	0.25	

Table B.4. continued.

Sources	Offset (arcmin)	¹² CO				¹³ CO			
		Flux (K km s ⁻¹)	Velocity (km s ⁻¹)	Width (km s ⁻¹)	T _L (K)	Flux (K km s ⁻¹)	Velocity (km s ⁻¹)	Width (km s ⁻¹)	T _L (K)
		12.01(0.11)	37.5	3.9	2.91	2.39(0.08)	37.2	2.8	0.81
		1.95 (0.11)	57.5	2.6	0.70				
	0, -20	12.94(0.11)	19.0	3.3	3.68	3.14(0.07)	18.7	2.2	1.36
		13.92(0.11)	29.8	15.2	0.86	2.27(0.16)	29.9	14.4	0.15
		3.05(0.11)	39.1	4.0	0.71	0.30(0.06)	39.1	1.7	0.17
		7.15(0.11)	58.2	12.0	0.56				
	10, -20	23.18(0.22)	21.6	6.9	3.18	3.56(0.11)	22.3	4.9	0.68
		13.37(0.27)	32.2	9.0	1.39	1.99(0.13)	32.0	7.4	0.25
		9.13(0.21)	57.8	9.4	0.91				
		6.54(0.17)	75.9	8.1	0.76				
	20, -20	13.37(0.41)	22.4	3.9	3.20	2.13(0.09)	22.8	2.9	0.69
		5.90(0.26)	30.3	3.0	1.85	1.15(0.09)	30.2	2.5	0.43
		9.81(1.44)	37.1	18.1	0.51				
		14.73(0.91)	56.7	12.3	1.13				
		11.37(0.20)	77.6	8.7	1.23				
	20, -10	1.39(0.18)	22.0	3.3	0.39				
		6.93(0.42)	33.0	11.1	0.59				
		3.69(0.30)	38.2	3.0	1.18	1.15(0.10)	36.6	5.5	0.20
		8.66(0.33)	56.3	6.4	1.27	0.78(0.09)	56.0	4.1	0.18
		5.92(0.47)	75.9	20.0	0.28				
	20, 0	3.48(0.31)	29.3	12.0	0.27				
		3.52(0.29)	38.4	4.6	0.73				
		10.75(0.16)	56.3	4.3	2.33	1.37(0.08)	57.0	3.8	0.34
	20, 10	6.17(0.62)	27.7	12.3	0.47				
		3.46(0.54)	35.5	4.6	0.70	0.47(0.09)	34.7	4.1	0.11
		6.71(0.19)	57.2	3.8	1.64	0.77(0.08)	57.5	3.0	0.24
	20, 20	3.39(0.41)	14.9	11.7	0.27				
		8.96(0.40)	33.0	12.0	0.70	0.55(0.10)	33.4	6.9	0.08
	10, 20	8.66(0.16)	27.0	16.4	0.50	1.14(0.11)	32.5	7.0	0.15
		14.00(0.16)	36.1	15.2	0.87				
		7.38(0.16)	56.1	6.1	1.13	0.57(0.09)	56.0	4.2	0.13
		2.17(0.16)	66.3	9.8	0.21				
	0, 20	6.04(0.13)	-0.1	8.3	0.69				
		7.81(0.13)	20.0	2.7	2.73	0.61(0.07)	19.8	1.8	0.32
		33.48(0.16)	34.5	22.5	1.40	2.15(0.19)	33.9	13.4	0.15
		11.20(0.16)	56.6	5.6	1.87	1.23(0.09)	56.5	4.5	0.26
	-10, 20	13.01(0.13)	20.5	2.8	4.45	2.02(0.08)	20.6	2.8	0.69
		17.64(0.13)	32.0	13.3	1.24	3.21(0.22)	31.6	9.9	0.30
		8.37(0.13)	42.5	5.2	1.51	1.83(0.18)	42.0	6.0	0.28
		8.51(0.13)	56.8	5.8	1.37	1.17(0.09)	57.6	5.1	0.21
		3.50(0.13)	72.9	9.4	0.35				
	-20, 20	2.84(0.18)	17.1	3.3	0.81	0.46(0.07)	16.8	2.0	0.22
		29.62(0.73)	29.7	14.6	1.91	6.21(0.27)	31.8	19.8	0.30
		13.54(0.65)	42.2	8.7	1.46	0.59(0.11)	41.0	2.6	0.21
		5.38(0.63)	58.1	9.5	0.53				
		6.09(0.54)	74.9	15.1	0.38				
	-30, 20	33.77(0.13)	30.6	16.5	1.92	1.03(0.06)	32.1	2.9	0.33
		11.66(0.13)	42.3	7.2	1.53	2.31(0.06)	41.4	4.5	0.48
		5.56(0.13)	47.9	3.7	1.41	1.05(0.06)	47.4	2.5	0.40
		4.76(0.13)	58.3	3.3	1.36				
		2.23(0.13)	78.8	8.0	0.26				
	-30, 10	17.47(0.99)	27.1	8.9	1.85	6.38(0.13)	28.8	7.5	0.79
		8.36(1.05)	30.9	4.5	1.73				
		22.39(0.28)	41.9	9.5	2.20	1.25(0.09)	40.2	1.8	0.64
	-30, 0	28.48(0.24)	27.1	10.6	2.52	5.61(0.15)	27.5	9.8	0.54
		18.91(0.10)	40.6	7.3	2.43	3.23(0.12)	40.4	6.2	0.49
		4.30(0.11)	59.9	2.4	1.68	0.63(0.05)	60.0	1.7	0.35
		1.38(0.12)	80.2	3.9	0.34				
	-30, -10	23.13(0.21)	22.1	8.2	2.64				

Table B.4. continued.

Sources	Offset (arcmin)	¹² CO				¹³ CO			
		Flux (K km s ⁻¹)	Velocity (km s ⁻¹)	Width (km s ⁻¹)	T _L (K)	Flux (K km s ⁻¹)	Velocity (km s ⁻¹)	Width (km s ⁻¹)	T _L (K)
		21.33(0.21)	29.8	9.2	2.19	9.17(0.11)	26.2	10.5	0.82
		29.58(0.21)	40.7	7.4	3.74	6.73(0.08)	40.6	5.7	1.11
		7.57(0.21)	60.3	3.5	2.03	1.59(0.05)	60.4	2.7	0.56
	-30, -20	33.81(0.23)	19.8	8.4	3.77	10.30(0.14)	23.3	12.7	0.77
		31.77(0.23)	31.5	14.1	2.12				
		23.18(0.23)	41.6	8.0	2.74	7.18(0.12)	40.4	8.4	0.80
		5.74(0.23)	58.4	6.1	0.89	0.58(0.08)	58.8	5.0	0.11
	-30, -30	41.81(0.25)	20.7	7.9	4.99	10.70(0.13)	20.9	6.4	1.57
		35.55(0.32)	35.0	12.6	2.65	5.78(0.16)	34.5	8.1	0.67
		9.17(0.21)	55.8	9.4	0.92	0.77(0.10)	56.5	3.9	0.18
		39.10(0.17)	19.9	6.2	5.94	10.40(0.14)	19.9	4.2	2.34
	-20, -30	24.55(0.26)	35.4	10.3	2.23	4.88(0.16)	35.8	5.6	0.83
		4.72(0.19)	51.3	9.5	0.47				
	-10, -30	27.52(0.31)	20.4	4.7	5.52	7.11(0.08)	20.5	2.9	2.31
		9.24(0.34)	37.3	5.1	1.70	1.28(0.10)	37.3	3.8	0.31
	0, -30	19.69(0.18)	19.9	4.9	3.77	4.12(0.12)	20.0	5.1	0.76
		4.77(0.26)	33.7	12.3	0.36				
		2.64(0.19)	55.0	9.4	0.27				
		3.39(0.16)	75.6	6.8	0.47				
	10, -30	13.66(0.18)	21.1	5.6	2.28	0.78(0.13)	19.9	1.4	0.51
		3.38(0.20)	33.9	8.5	0.37				
		3.62(0.18)	58.5	6.9	0.50				
		5.44(0.20)	77.9	7.8	0.66				
	20, -30	5.58(0.08)	23.0	4.2	1.24	0.70(0.09)	22.9	2.5	0.27
		5.81(0.08)	31.1	3.3	1.66	0.59(0.08)	30.6	2.1	0.26
		11.94(0.08)	56.7	12.5	0.90				
		8.37(0.08)	79.2	9.4	0.83				
	20, 30	9.61(0.79)	19.4	15.5	0.58				
		13.84(0.94)	35.7	13.2	0.98	0.82(0.13)	35.3	5.5	0.14
		3.43(0.55)	55.0	10.2	0.32				
	10, 30	13.60(0.19)	26.8	18.2	0.70				
		11.92(0.19)	36.3	10.0	1.12	2.31(0.19)	34.1	9.0	0.24
		7.57(0.19)	44.7	5.7	1.25	0.82(0.11)	45.4	3.9	0.20
		5.64(0.19)	57.1	4.4	1.21	0.79(0.10)	56.5	3.6	0.20
	0, 30	7.02(0.17)	-2.6	6.5	1.02				
		1.33(0.08)	15.8	1.7	0.76				
		17.10(1.12)	28.6	23.7	0.68				
		21.53(0.96)	40.7	10.1	2.01	4.87(0.16)	38.9	11.2	0.41
		9.17(0.15)	57.6	5.0	1.74	1.72(0.13)	57.1	4.8	0.34
	-10, 30	1.97(0.12)	20.8	2.7	0.69				
		17.89(0.12)	30.1	10.0	1.68	4.25(0.55)	31.5	11.9	0.34
		18.21(0.12)	40.9	9.1	1.87	2.40(0.53)	40.8	7.2	0.31
		7.86(0.12)	57.9	4.9	1.52	1.01(0.10)	58.8	4.3	0.22
		5.54(0.12)	71.7	10.2	0.51				
	-20, 30	15.92(0.49)	23.1	10.2	1.46	0.79(0.12)	16.4	1.8	0.43
		16.35(0.74)	31.4	5.2	2.95	4.32(0.26)	31.3	3.5	1.15
		18.33(0.49)	40.6	10.8	1.59	1.88(0.38)	40.9	4.7	0.38
		6.08(0.19)	59.3	4.9	1.16				
		4.77(0.18)	77.8	5.1	0.88				
	-30, 30	2.78(0.18)	15.6	2.0	1.30	1.08(0.10)	15.9	2.1	0.49
		22.00(0.36)	31.2	6.4	3.25	6.06(0.18)	31.4	3.8	1.48
		16.81(0.41)	44.7	10.0	1.58	4.42(0.26)	43.3	11.4	0.37
		2.90(0.21)	57.4	3.0	0.90	0.84(0.11)	57.6	2.4	0.33
		1.59(0.19)	74.4	5.0	0.30				
	-40, 30	22.17(1.59)	31.3	7.3	2.85	6.50(0.38)	31.2	7.5	0.81
		17.26(2.04)	45.9	14.9	1.09				
		4.52(0.76)	67.3	3.9	1.09				
	-40, 20	17.56(0.69)	25.9	5.6	2.97	4.03(0.19)	25.8	4.1	0.93
		14.01(0.79)	32.4	4.1	3.25	2.90(0.19)	32.6	3.5	0.78

Table B.4. continued.

Sources	Offset (arcmin)	¹² CO				¹³ CO			
		Flux (K km s ⁻¹)	Velocity (km s ⁻¹)	Width (km s ⁻¹)	T _L (K)	Flux (K km s ⁻¹)	Velocity (km s ⁻¹)	Width (km s ⁻¹)	T _L (K)
		9.13(0.92)	39.1	4.5	1.91	1.58(0.19)	39.3	3.0	0.49
		11.84(0.82)	48.0	7.5	1.49	2.35(0.23)	48.5	5.7	0.39
		2.60(0.40)	68.2	3.4	0.71				
	-40, 10	37.98(0.95)	28.1	9.5	3.74	12.10(0.24)	28.3	6.6	1.73
		32.06(1.09)	43.1	12.0	2.50	4.61(0.49)	43.6	10.1	0.43
						1.21(0.17)	40.4	1.6	0.72
						1.09(0.31)	50.5	3.3	0.31
	-40, 0	36.61(1.09)	27.4	11.4	3.02	6.91(0.37)	27.6	7.5	0.86
		32.74(0.96)	40.7	6.8	4.53	8.42(0.33)	40.2	5.6	1.43
		5.00(0.77)	57.8	6.6	0.71				
	-40, -10	41.92(0.48)	25.7	9.8	4.00	6.74(0.23)	25.8	7.1	0.90
		46.00(0.44)	40.7	8.4	5.16	9.56(0.22)	40.6	6.4	1.41
		15.80(0.31)	59.2	5.3	2.81	2.03(0.17)	59.1	4.1	0.47
	-40, -20	43.86(0.46)	22.7	10.7	3.87	6.95(0.26)	23.3	8.0	0.82
		46.89(0.48)	40.0	10.8	4.08	8.62(0.26)	39.5	8.2	0.99
		8.88(0.27)	57.8	5.0	1.67	1.36(0.17)	57.7	4.2	0.31
	-40, -30	35.64(0.54)	21.6	9.0	3.71	7.53(0.25)	22.5	8.6	0.82
		37.23(0.65)	37.0	12.8	2.72	1.06(0.14)	34.6	1.7	0.58
		3.180(0.37)	56.5	6.1	0.49				
	-40, -40	42.51(1.75)	19.6	6.5	6.18	8.34(0.59)	19.2	3.4	2.32
		43.94(2.19)	34.4	13.3	3.10	11.70(0.99)	33.5	14.7	0.75
	-30, -40	46.68(1.29)	20.5	7.0	6.25	12.40(0.42)	20.1	4.0	2.96
		39.34(1.64)	33.7	14.5	2.55	10.50(0.68)	29.4	20.0	0.50
		6.37(0.76)	54.5	8.7	0.69				
	-20, -40	56.25(0.63)	19.7	9.1	5.82	15.90(0.36)	20.7	4.8	3.16
		15.00(0.70)	37.2	9.1	1.55				
		5.51(0.67)	52.5	6.5	0.79				
	-10, -40	24.58(0.63)	20.1	4.9	4.76	4.31(0.19)	20.2	2.7	1.52
		5.97(0.69)	40.8	7.9	0.71				
		5.28(0.64)	57.2	7.7	0.64				
	0, -40	3.12(0.30)	15.2	2.3	1.25				
		7.67(0.36)	19.9	3.3	2.18	0.98(0.28)	19.7	4.2	0.22
	10, -40	1.39(0.12)	15.9	1.3	1.02				
		7.99(0.12)	21.0	4.4	1.71	0.98(0.32)	20.9	5.1	0.18
		4.94(0.12)	61.6	7.0	0.66				
	20, -40	1.32(0.21)	14.4	1.9	0.66				
		5.91(0.53)	57.2	9.5	0.58				

Notes. Parameters listed concern the simultaneously observed ¹²CO and ¹³CO emission line. The ¹²CO and ¹³CO line velocities uncertainty together are about 0.2 km s⁻¹ and the line width uncertainty together are about 0.2 km s⁻¹.